

Effect of Trailing Edge and Span Morphing on the Performance of an Optimized NACA6409 Wing in Ground Effect

 **Dominic Clements** [AQ1](#)

Aero, Astro and Comp Engineering, University of Southampton, Southampton, UK, [\[Please add in post code SO16 7QF\]](#) UK e-mail: drc1n18@soton.ac.uk

Kamal Djidjeli

Aero, Astro and Comp Engineering, University of Southampton, Southampton, UK, [\[Please add in post code SO16 7QF\]](#) UK e-mail: kkd@soton.ac.uk

Contributed by the Fluids Engineering Division of ASME for publication in the JOURNAL OF FLUIDS ENGINEERING. Manuscript received March 28, 2024; final manuscript received August 28, 2024; published online xx xx, xxxx. Assoc. Editor: Yang Liu.

Abstract

A computational fluid dynamics (CFD) investigation was carried out on a three-dimensional NACA6409 wing in ground (WIG) effect at a Reynolds number of 320,000. Using a multi-objective-SHERPA algorithm, a root angle of 4 deg angle of attack, a tip angle of 6 deg, a forward sweep, and a tip chord of 20% of the root chord produced an optimum aerodynamic efficiency across all ground clearances. Optimization showed a gain in aerodynamic efficiency of 41% at $h/c = 0.05$ ground clearance and a 31% gain at $h/c = 0.2$ compared to a rectangular planform wing. Next, fish bone active camber (FishBAC) morphing was applied to the optimized wing varying the morphing start locations along the chord at both the tip and root. A later start location produced the highest aerodynamic efficiency but increased manufacturing complexity. Extendable span morphing was also tested and was found that increasing the span from $1c$ to $1.5c$ increased the aerodynamic efficiency of the optimized wing by 27.4% at $h/c = 0.1$. Varying the span from $0.8c$ to $1.2c$ in ground effect had a small effect on the drag for small ground clearances; for large ground clearances, the total drag

decreased as the span increased. Smaller gains were seen when the span morphing was applied to the rectangular wing. The FishBAC morphing was applied in the spanwise direction to morph the wingtip, sealing the flow beneath the wing. Also, the proportion of the morphing wingtip caused the trailing edge to be closer to the ground further enhancing ground effect.

1 Introduction

The aerodynamic performance of a wing can be enhanced by flying in proximity to the ground known as ground effect; the analysis of wings in ground in effect is typically split into two areas known as chord-dominated and span-dominated ground effect [1]. The chord-dominated performance gains are associated with a two-dimensional airfoil profile, and the span is associated with a three-dimensional wing. First, looking at the chordwise enhancement, which is mainly associated with lift gains, is due to the fixed trailing edge condition imposed by the Kutta condition causing all effects from the ground to be seen upstream of the trailing edge beneath the airfoil [2,3]. When a wing is brought into ground effect, the pressure on the lower surface of the wing increases, resulting in an increase in lift. Second, when a wing is brought into ground effect, a spanwise enhancement can be seen, where the wingtip vortices are pushed outboard of the wing, reducing the induced drag [4–9].

For some airfoil profiles in ground effect, the lift can be reduced as a wing is brought into ground effect and in some cases of airfoil geometry and angle of attack (AoA) [10,11]. This occurs when the airfoil's lower surface is closer to the ground than the distance between the trailing edge and the ground. A wing is typically considered to be in freestream when the ratio between the ground clearance and chord is 1, and below $h/c = 0.4$ the ground effect becomes more prominent [1,12]. By reducing the ground clearance, the lift increases at a greater rate as the wing becomes closer to the ground. This poses a problem for wings in ground effect where the variation in lift will cause large stability issues problems due to variations in the pitching moment [10,13], making wing in ground effect vehicles extremely sensitive to flying in ground effect.

Wings in ground effect are typically used in ~~in-to~~ marine applications, ~~craft~~, allowing ~~craft them~~ to fly above the water surface to increase their speed and reduce the drag caused by the highly dense water compared to air, thereby reducing fuel consumption. In the 1960s, wing in ground effect crafts

were heavily researched [1], however, due to instability issues making the craft difficult to fly in ground effect, the craft did not gain popularity. A major problem with the early craft was the size of the craft and the large amounts of fuel required to achieve the intended flight speed. Modern day wing in ground effect vehicles are typically much smaller being designed as small passenger craft. A typical example of this is the Airfish, which can carry up to eight people [14].

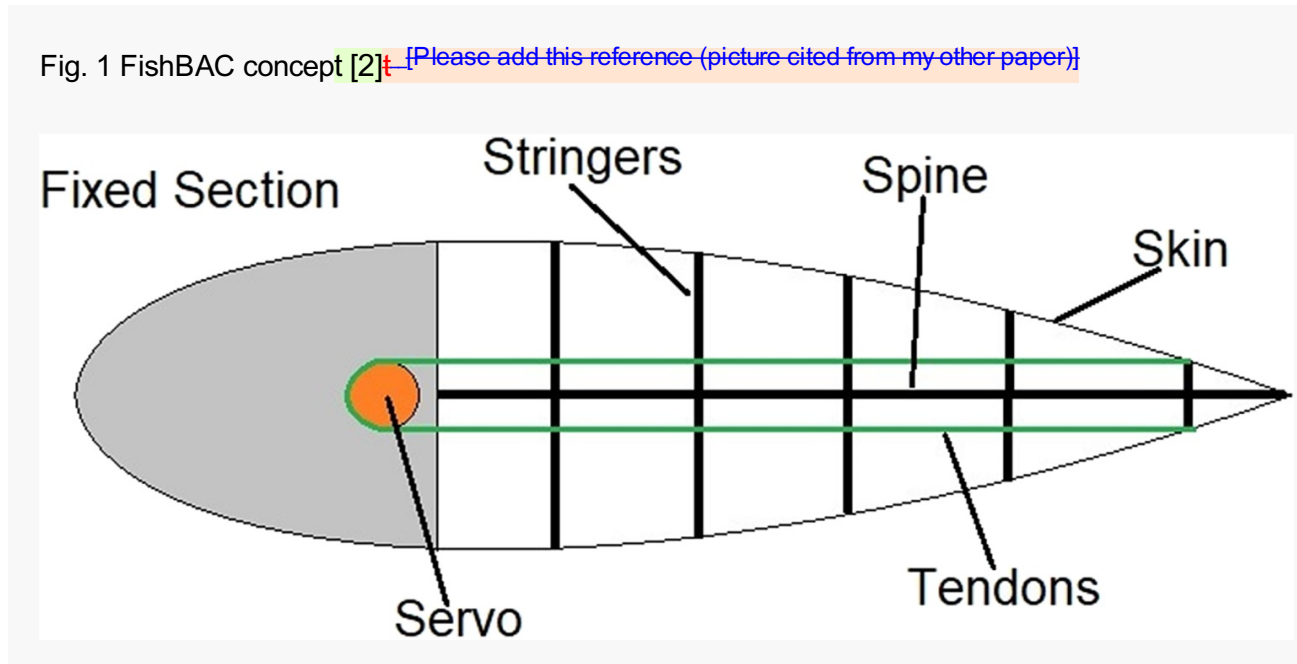
There are many different methods of morphing wings; these may include twist, sweep, chord length, camber thickness, span bending, span twisting, camber, and span extension morphing [15,16]. Due to the large number of morphing techniques, the type of morphing needs to be selected based on the feasibility of implementing the design, cost, weight gain, and space required to house the mechanisms [15,17]. Span-extending morphing allows the aspect ratio of a craft to be adjusted; a higher span typically increases aerodynamic efficiency [18,19], however, reduces roll rates and can make maneuverability difficult such as taxiing around airports. A higher span also allows the craft to fly at a lower speed [20]; therefore, extending the span allows for a wide range of operating conditions.

The low aspect ratio of wings in ground effect often has a large negative effect on aerodynamic performance, and studies have investigated the use of wingtips to seal the lower surface [6,9,13,21]. However, it is difficult to fly close to the ground safely especially flying over water without a wingtip touching the ground. Tiltable wingtips are an alternative to end wing end plates which effectively hinge the wingtip geometry downwards to seal the lower surface which offers significant performance gains by controlling the wingtip vortex [9].

Camber morphing airfoils allow the variation of lift of a wing and typically replace the control surfaces on an aircraft. This has the advantage of eliminating the gap between the wing and control surface itself, which increases efficiency [22] and allows smaller trailing edge deflection for the same amount of roll when compared to a traditional flap control surface [23]. A study by Woods and Friswell [24] introduced fish bone active camber (FishBAC) demonstrated by the schematic (Fig. 1), which morphs the camber of the airfoil by defining the curve and the morphing mechanisms. The FishBAC morphing was bio-inspired to allow large deflections of a camber morphing airfoil. Figure 1 shows a schematic of this structure consisting of a spine which was deflected at the trailing edge by a servo

and a belt. The airfoil surface was an **EMC** skin membrane with the shape of the surface defined by stringers. [AQ2](#)

Fig. 1 FishBAC concept [2]. [\[Please add this reference \(picture cited from my other paper\)\]](#)



To the best of the authors' knowledge, there is very little work combining the two areas of morphing wings and wings in ground effect. In previous work [2], morphing wings were applied to a two-dimensional NACA6409 airfoil. The work presented in this study extends this to three dimensions. Due to the large number of variables of the wing including the tip chord, angle, sweep, and root angle of attack, an optimization study was first carried out and compared to a baseline rectangular wing before applying camber, span extension, and wingtip morphing techniques.

2 Methodology

This study used computational fluid dynamics (CFD) to investigate the optimization of a three-dimensional wing in ground effect and the morphing of the three-dimensional wing in ground effect. Reynolds-averaged Navier–Stokes modeling was used in this study with the k -Omega SST turbulence model at a Reynolds number of 320,000 based on the chord length. The simulations in this study were run until the residuals had reached a magnitude of 10^{-4} and that the lift and drag had

converged. The converged simulations yielded a y^+ of approximately 1 as recommended in the user manual for the CFD software [25] for the particular turbulence model used.

First, in this study, an optimization study was carried out using the built-in Design Manager in the star ccm+ software to perform a multidisciplinary design optimization. The optimization study was carried out due to the large number of variables of a three-dimensional wing including twist, sweep, and taper of the wing as well as root and tip angles of attack. Starting with a rectangular wing with a NACA6409 profile and aspect ratio of 2, a parametric model was created in star ccm+ to vary the parameters listed in Table 1. Five different ground clearances were tested at $h/c = 0.05, 0.1, 0.2, 0.4,$ and 1 , which are nondimensionalized with the airfoil chord. The twist of the wing was carried out by independently varying the root (θ_r) and the tip (θ_t) angle of attack. The sweep of the wing was varied by adjusting the value of t/c , the dihedral by adjusting d/c , and the tip chord by adjusting tc as shown in Fig. 2. The range of parameters tested can be seen in Table 1.

Fig. 2 Input parameters for parametrization

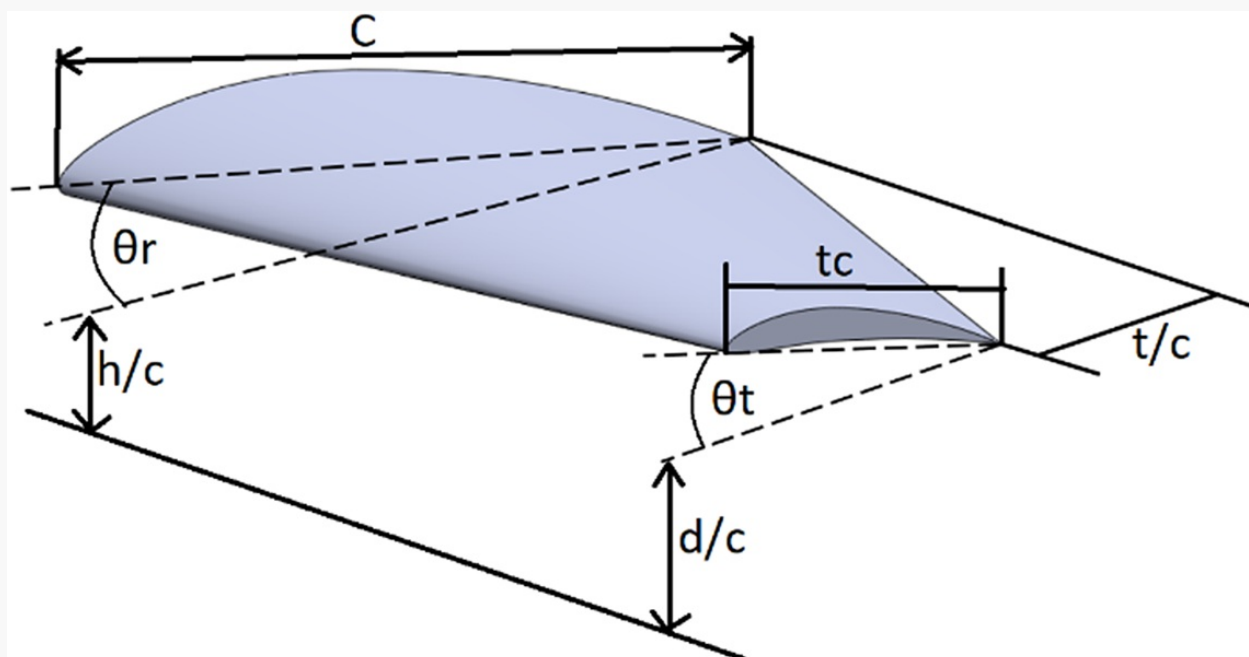


Table 1 Input parameters for parametrization

Parameter	Notation	Range	Increment
Root angle	θ_r	[2.0, 8.0] deg	1.0 deg
Tip angle	θ_t	[0.0, 8.0] deg	1.0 deg
Tip chord	tc	[20, 100] %c	20% root chord
Tip height	d/c	[0, 40] %c	20% root chord
Tip position	t/c	[0, 80] %c	20% root chord

The overall objective for the optimizations was to improve the aerodynamic efficiency which was achieved by setting the lift goal to maximum and drag to minimum. A total of 200 design iterations were performed using the multi-objective-SHERPA algorithm within Design Manager.

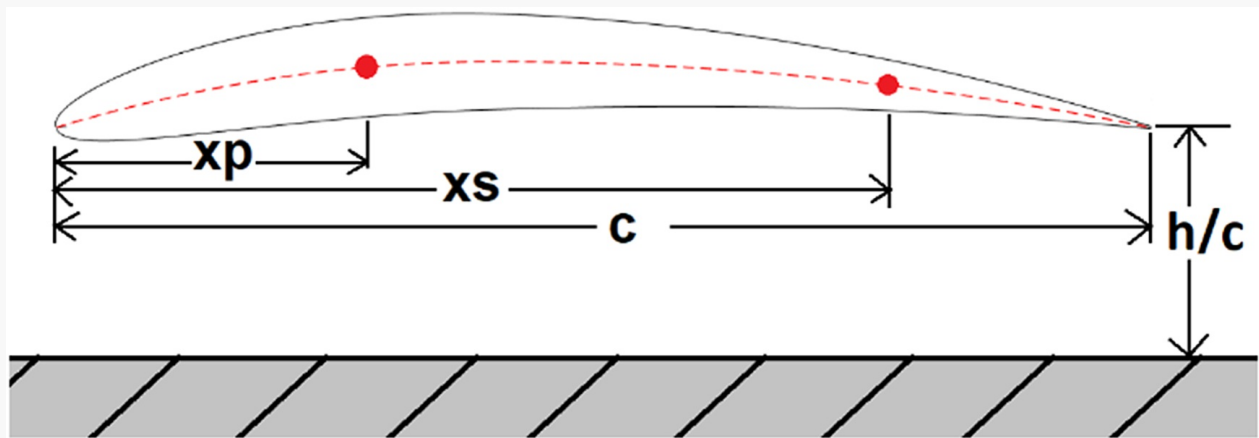
Next, static morphing of the optimized wing was carried out by using the FishBAC morphing method. In this study, static morphing is performed by running steady-state simulations with the geometry swapped out with the different morphed configurations. This provides an initial analysis without the extra complexity of modeling in time and extra computational expense in order to provide an initial understanding of a morphed three-dimensional wing in ground effect. Three separate studies were carried out including FishBAC, extendable span, and wingtip morphing.

The NACA6409 is a cambered airfoil, where the geometry of the airfoil can be split into a camber line (Eq. (2)) with varying thickness (Eq. (1)) applied around this line to define the airfoil surface [24]. The thickness is applied using two separate equations, one for the leading edge up to the point of maximum airfoil thickness (x_p in Fig. 3) and one for the distance between x_p and the trailing edge with (t_a) the airfoil maximum thickness. To morph the airfoil, a third equation was defined at a morphing start location (x_s) along the chord defined by (Eq. (2)). In three dimensions, the start location and displacement were varied independently at the wing root and tip. In these equations, c is the airfoil chord, w_{te} is the trailing edge deflection, m is the maximum airfoil thickness, and x_p is the location of the maximum airfoil thickness from the leading edge

$$y_t = 5t_a(0.2969\sqrt{x/c} - 0.126(x/c) - 0.351(x/c)^2 + 0.2843(x/c)^3 - 0.1015(x/4)^4) \quad (1)$$

$$y_c = \begin{cases} \frac{mx}{x_p^2} \left(2x_p - \frac{x}{c} \right), & 0 \leq x < x_p \\ \frac{m}{1-x_p^2} \left(1 - 2x_p + 2x_p x - x^2 \right) & x_p < x < x_s \\ \frac{m}{1-x_p^2} \left(1 - 2x_p + 2x_p x - x^2 \right) + \frac{W_{te}(x-x_s)^3}{(1-x_s)^3} & x_s < x \leq c \end{cases} \quad (2)$$

Fig. 3 Airfoil point location definitions



3 Mesh Independence and Validation

Computational fluid dynamics was carried out in this study to obtain data and to ensure that the mesh and physics within the CFD were set up correctly. Validation was carried out using a mesh independence study and comparing the simulations with existing data. First, a mesh independence study was carried out to ensure that the cell size was adequate to capture the flow details and not influence the data. The mesh size was varied by varying the mesh base size which scales the mesh and refinement areas. A fixed boundary layer height of 0.02% chord was used to ensure that the y^+ remained fixed at 1 as recommended in the CFD user manual [25] for the turbulence model. The NACA6409 rectangular wing with an aspect ratio of 2 was used for the mesh independence at a ground clearance of $h/c = 0.1$ and an angle of attack of 4 deg. The discretization error due to grid

convergence was determined using the ASME V&V 20 Committee [26]. Three mesh refinements were carried out using fine, medium, and coarse meshes as shown in Table 2.

Table 2 Mesh size lift and drag values for a NACA6409

Mesh refinement	Cell count	C_l	C_d
Fine	74,121,642	0.708	0.0489
Medium	20,017,574	0.712	0.0492
Coarse	6,178,815	0.724	0.0500

The values of lift and drag coefficients at zero grid spacing are determined using the Richardson extrapolation by applying the two finest grids in Eq. (3), where f defines the coefficients of the fine medium and coarse meshes. The subscripts f , m , and c denote the fine, medium, and coarse meshes, respectively. The order of convergence is defined by $p = (\ln(f_c - f_m)/(f - f_f))/\ln(r)$, where r is the refinement ratio with $r = 2$ as traditionally used [26]

$$p_r = \frac{f_r + (f_f - f_c)}{(r^p - 1)} \quad (3)$$

The theoretical zero grid spacing lift value for $C_l = 0.706$ and drag $C_d = 0.0487$. The grid convergence index (GCI) defined in Eq. (5), with a safety factor of $F_s = 1.25$ for comparison over three grids [26], and the relative error defined as $\varepsilon = (f_f - f_m)/f_f$ using the fine and medium meshes, and $\varepsilon = (f_m - f_c)/f_m$ for the medium and coarse meshes. For the lift, this yielded a GCI = 0.3701% for the fine and medium meshes and a GCI = 1.063% for the medium and coarse meshes. For the drag, a GCI = 0.4562% for the fine and medium meshes and a GCI = 1.0823% for the medium and coarse meshes

$$\text{GCI} = \frac{F_s |\varepsilon|}{(r^p - 1)} \quad (4)$$

The solution is then checked with Eq. (5) to ensure that it falls within the asymptotic range of convergence. A convergence value of 0.9944 for the lift and 1.0573 for the drag, which is close to 1, shows that it was within the convergence range [AQ3](#)

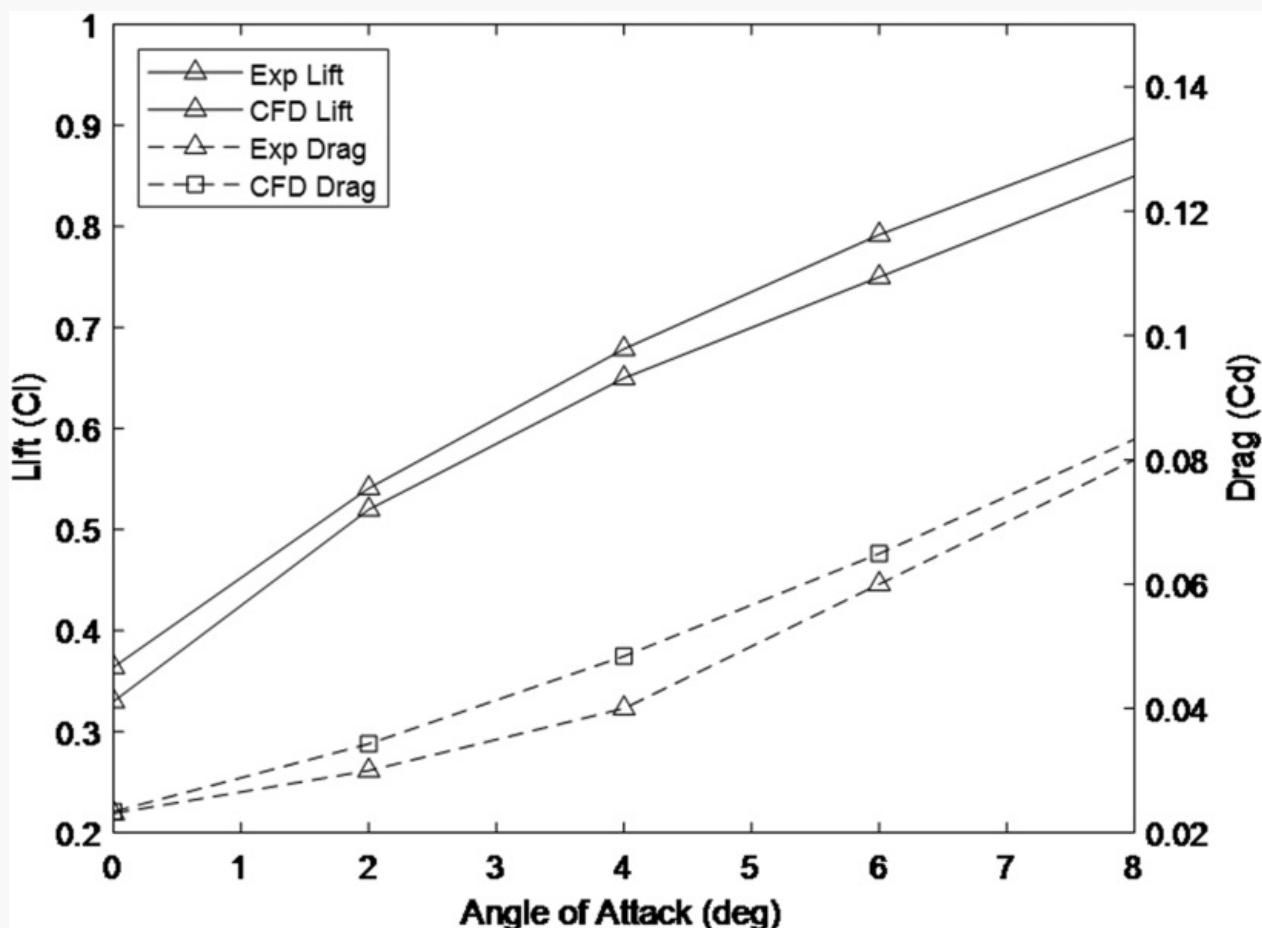
$$\mathbf{1} = \frac{GCI_{fm}}{r^p GCI_{mc}} \quad (5)$$

The error between the theoretical zero grid spacing and the mesh refinements is shown in Table 3 for the lift and drag coefficients. It was found that the coarse mesh has a 2.56% error for the drag and a 2.42% error for the lift, showing that the mesh is size-dependent. The medium mesh has a 0.85% error for the lift and 0.97% for the drag, and the fine mesh has a 0.3% error for the lift and 0.36% for the drag. The fine mesh was selected and used as it has a lower error and gives values closer to the theoretical zero grid spacing.

Table 3 Mesh refinement error

Mesh refinement	C_l error%	C_d error%
Fine	0.30	0.36
Medium	0.85	0.97
Coarse	2.42	2.56

To validate the results, a comparison was made between the mesh and published experimental data [6] for the NACA6409 at $h/c = 0.1$ ground clearance shown in Fig. 4. The experimental data used a Reynolds number of 345,000, and comparisons were made against the aspect ratio of 2 wing as used in this study. The lift and drag for both the fine mesh and experimental data are shown in Fig. 4. The lift showed a minimum difference of 4% and a maximum difference of 5% when comparing the experimental literature data with the CFD carried out in this study. The drag showed a difference of 4.1% at 8 deg angle of attack and a 5.8% difference at 0 deg angle of attack when comparing the drag between the experimental and CFD. Both the lift and drag showed very similar trends when comparing the experimental to the CFD data. The experimental drag was slightly higher than the CFD due to the slightly higher separation on the upper surface which corresponded to the slightly higher lift for the CFD and the fact that the drag was of smaller magnitude compared to the lift; therefore, the error for the drag in the CFD was greater compared to the lift.

Fig. 4 Lift and drag of fine mesh compared to experimental data at $h/c = 0.1$ 

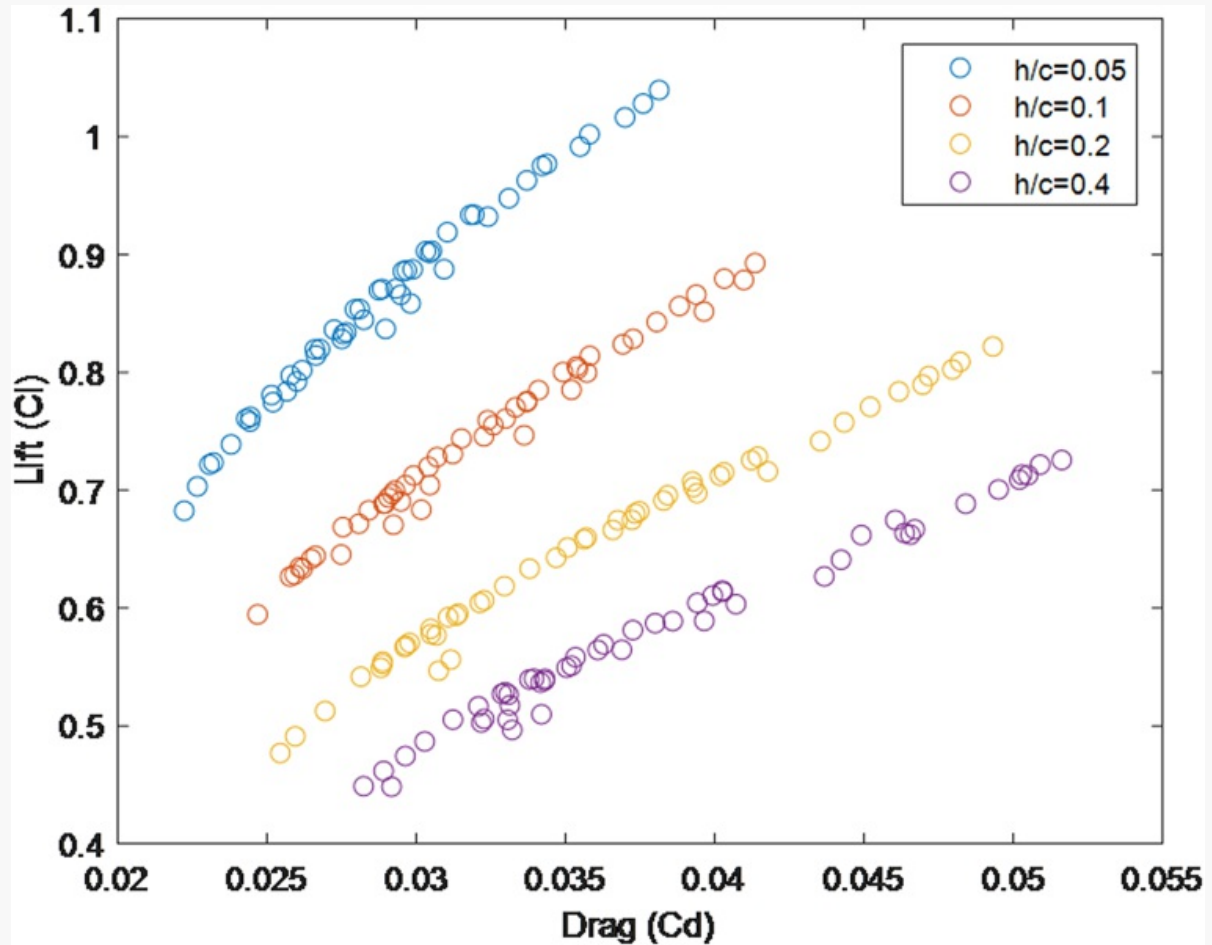
Although there were differences between the CFD and experimental data, these differences can be explained by the CFD errors and the uncertainties within the experiment. One difference between the experimental and CFD was that the CFD used a tangential velocity vector to simulate a moving ground, whereas the experiment had a stationary ground. This is the main reason why the difference between the experiment and CFD is greater at lower ground clearances. This was highlighted by Yang et al. [27] who compared stationary and moving grounds.

4 Results and Discussion

4.1 Three-Dimensional Wing Optimization.

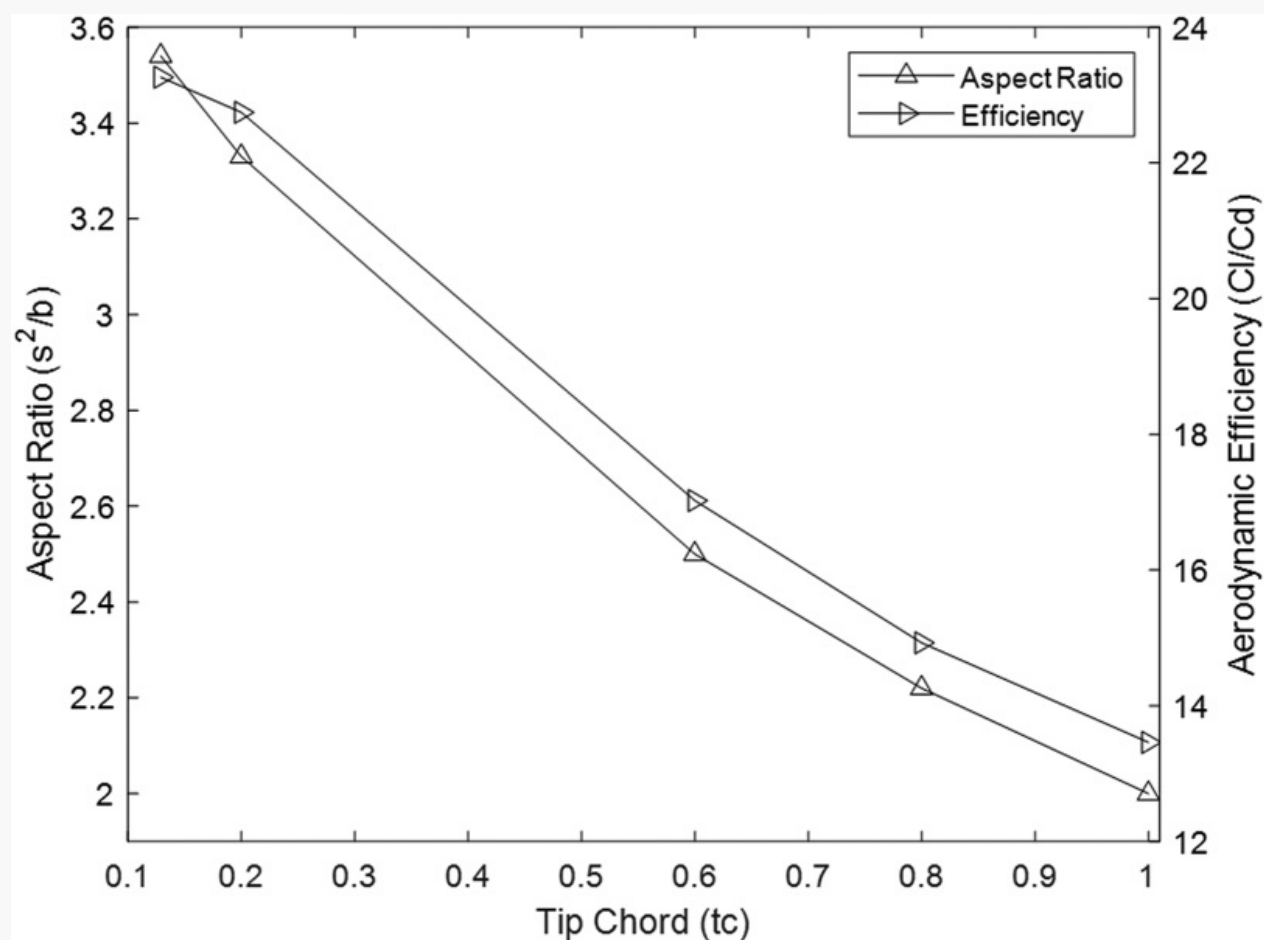
An optimization study was carried out **varying using** the parameters in **Table ??** **Fig. 2** for each ground clearance, resulting in a total of five optimization studies. **AQ4** The studies carried out produced a Pareto front for each ground clearance, seen in Fig. 5, showing all the optimum designs with equal performance. A design can then be selected from these fronts based on the requirements of the aircraft design; however, having run five design sets, a crossover in designs can be sought to ensure optimum performance across the ground clearance variation. Although the effects of sweep, tip chord, twist, and dihedral have been investigated [28], this study extends that research by investigating multiple ground clearances and by adjusting all of these parameters simultaneously to find the best possible solutions on a Pareto front.

Fig. 5 Pareto front for each ground clearance NACA6409 wing



It was observed that the optimal designs on the Pareto front had a wingtip chord of $0.2c$ with the tip profile trailing location of $0.8c$ ahead of the root trailing edge where c is the root chord length. A smaller wingtip chord effectively increases the aspect ratio of the wing. The aspect ratio ($AR = b^2/A$) was plotted for decreasing the wingtip chord in Fig. 6. Wings in ground effect typically have low aspect ratios to prevent rolling restrictions of the craft. With the higher aspect ratio wing, the aerodynamic efficiency can be improved, and increasing the aspect ratio by a small amount on a low aspect ratio wing as seen in this study dramatically increases the aerodynamic performance, as also seen by Jung et al. [6] and Fink and Lastinger [29].

Fig. 6 Effect of wingtip chord on aerodynamic efficiency and aspect ratio at 4 deg root, 6 deg tip AoA, and $h/c = 0.1$



The lower surface pressure of the wing was analyzed (Fig. 7) by varying the tip chord for a root angle of 4 deg and a tip of 6 deg angle of attack in 10% ground effect. [AQ5](#) This study focuses on the wing's lower surface pressures which are directly affected by the ground effect, while the upper surface was found to have much smaller variations from ground effect. In general, an increase in pressure on the lower surface increased pressure on the upper surface, and a decrease in pressure on the lower surface resulted in a decrease in pressure on the upper surface. Although both the upper and lower surface pressures would vary, the upper surface would vary by a much smaller amount compared to the lower surface making the lower surface pressure effects dominant. Initially,

the lower surface high-pressure region (Fig. 7) extended along the span as the wingtip chord was reduced from 100% to 60%, which resulted in an increase in lift seen in the lift plot Fig. 8. Reducing the tip chord from 60% to 20% caused the high-pressure region to be pushed further toward the wingtip, but reduced the magnitude of the pressure coefficient across the entire lower surface, thus reducing the overall lift. Reducing the tip chord further from 20% to 13% of the root chord showed that the high-pressure region on the lower surface became smaller, which explains the sharp reduction in lift seen in Fig. 8 between 20% and 13% tip chord. As the lift decreased, the drag decreased at a higher rate, which caused the aerodynamic efficiency to increase as the wingtip chord decreased, as shown in Fig. 6. Below 20%, the lift decreased at a similar rate to the drag, causing the aerodynamic efficiency to increase by a minimal amount. The lift decreased as the tip chord was reduced due to the chord reducing along the span. The ground clearance was defined as the ratio of height to wing chord, and as the chord decreased along the span, this ratio increased along the span, and increasing the h/c ratio was seen to reduce the lift.

Fig. 7 Wing sweep lower surface pressure for tip chords of 100%, 60%, 20%, and 13% in ground effect ($h/c = 0.1$) and 4-deg root AoA and 6-deg tip AoA

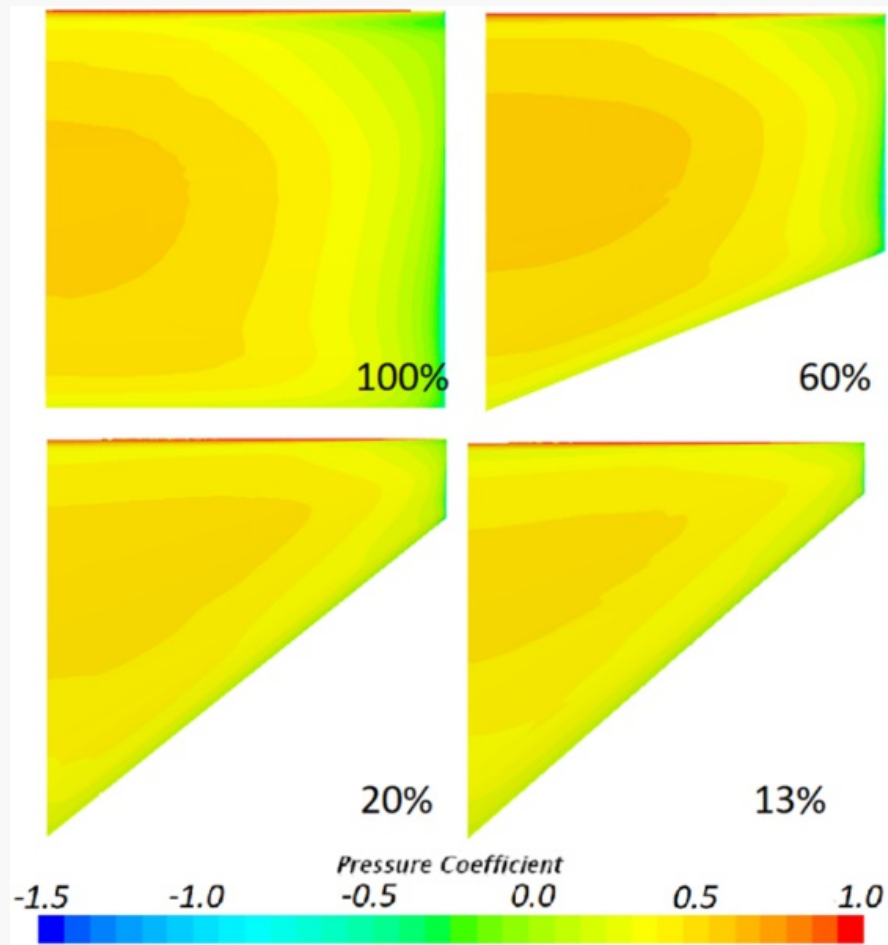
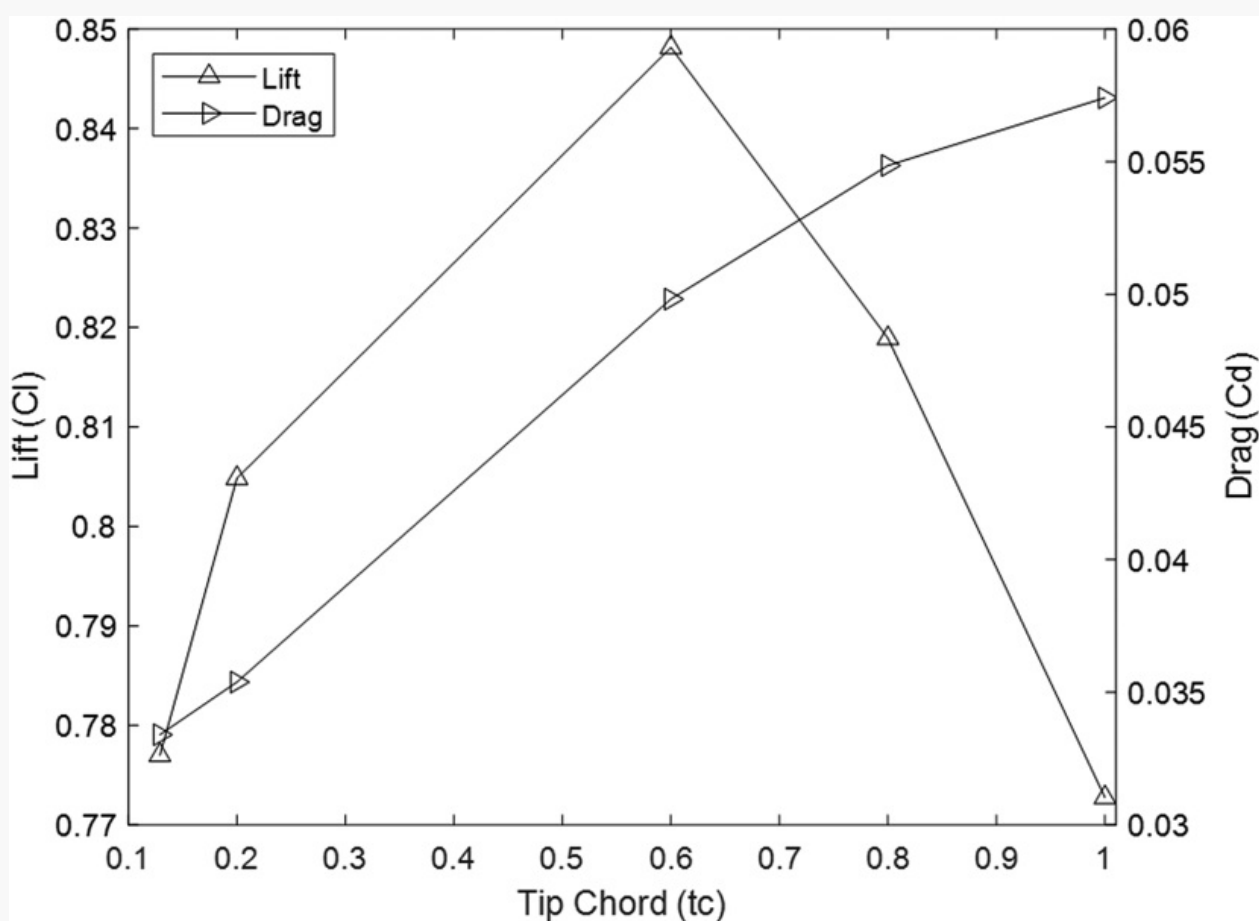
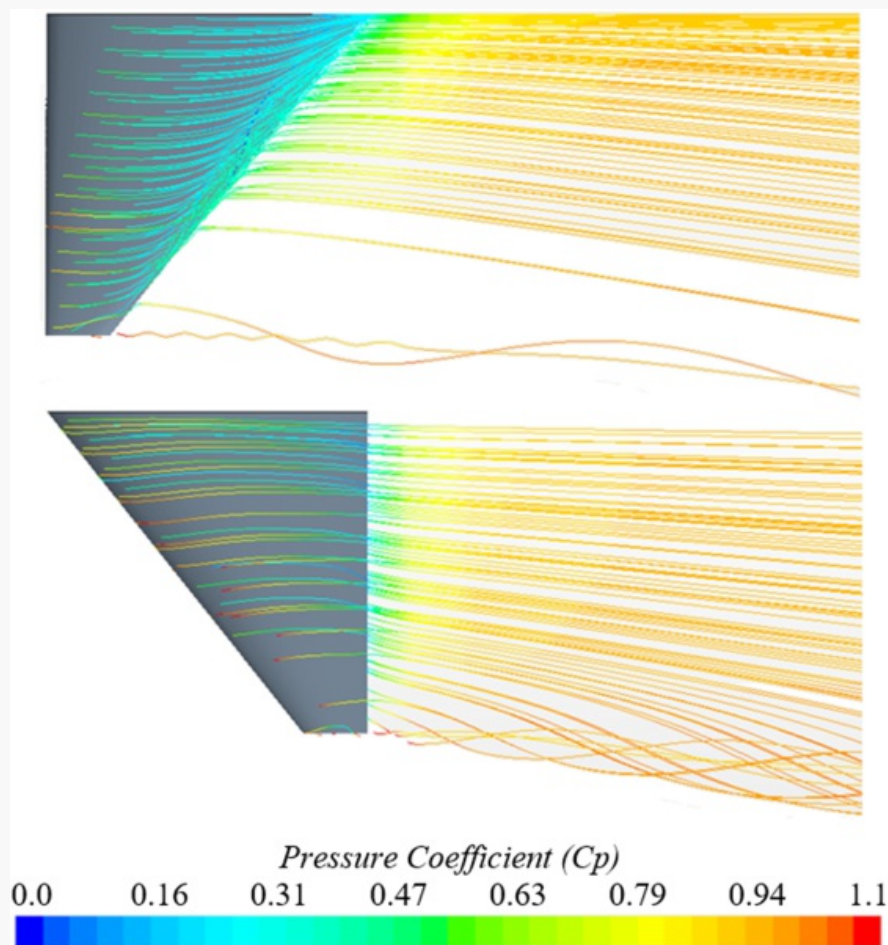


Fig. 8 Wingtip chord sweep for root at 4 deg root, 6 deg tip AoA, and $h/c = 0.1$ 

For the 20% tip chord, the wing had a forward sweep with the leading edge perpendicular to the root chord. This resulted in a distance of 80% where the wingtip was moved forward. This was seen to be due to the sweep of the wing affecting the wingtip vortex. Analyzing the wingtip vortex streamlines showed that the streamlines left the trailing edge normal to the trailing edge near the root, downstream the streamlines were curved outwards in the direction of the wingtip (Fig. 9 lower). The forward sweep showed the streamlines flowing downstream along the trailing edge (Fig. 9 upper). This showed that the rear swept wing was feeding the wingtip vortex, which reduced the overall aerodynamic performance of the wing.

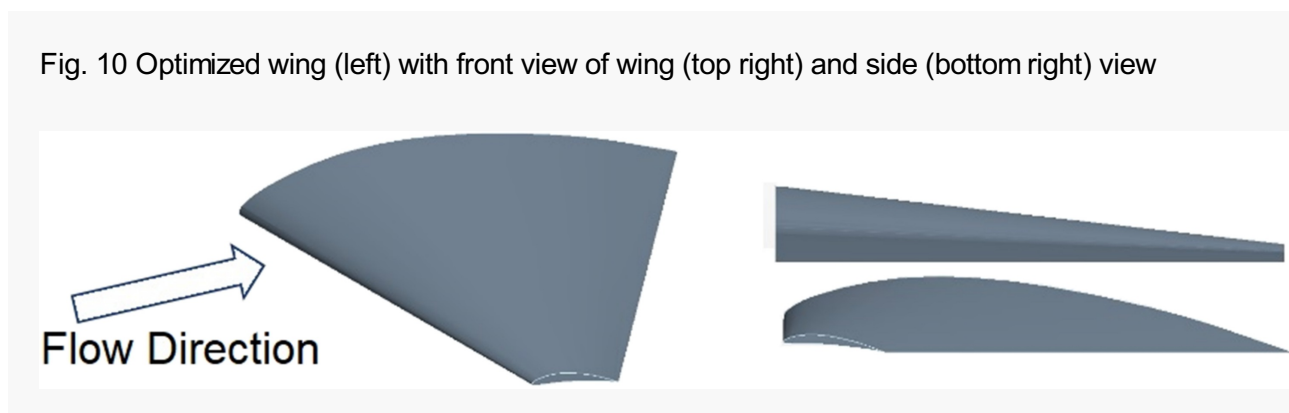
Fig. 9 Streamlines of forward (top) and rear (lower) sweep wing



The angle of the root was found to have a significant effect on the performance of the wing. Analyzing the different designs showed that a root angle of attack between 2 deg and 4 deg had the highest performance. Higher root angles produced higher overall lift but reduced the aerodynamic efficiency of the wing. This was due to the higher root angle causing a higher pressure on the lower surface at the wing root. The flow vector in the plan view of the wing (Fig. 9) can be split into streamwise and spanwise directions with the streamline being the resultant vector. With the pressure of the wingtip fixed by the wingtip vortex, the higher pressure at the root resulted in a greater spanwise flow which fed the wingtip vortex and caused an increase in aerodynamic drag. The tip

angle was found to have little effect on the wing performance over the range of angles tested. This showed that the spanwise flow vector had a greater influence on the performance of the wing than the increased induced drag.

Analysis of all the designs on the Pareto front has shown that different ground clearances produced different optimal designs and that there is no single design that is optimal across the range of ground clearances. Therefore, a compromise is made to select the best-performing wing across the range of ground clearances. It was found that in freestream the optimized wing was completely different from the wings in ground effect; therefore, the best performing wing in ground effect was selected comparing the wings up to $h/c = 0.2$ clearance as this study focused on ground effect. Figure 10 shows the geometry of the selected optimized wing which has a tip position of $0.8c$ upstream of the root trailing edge and a chord of $0.2c$. The root angle of attack was 4 deg, and the tip angle was 6 deg with no dihedral.



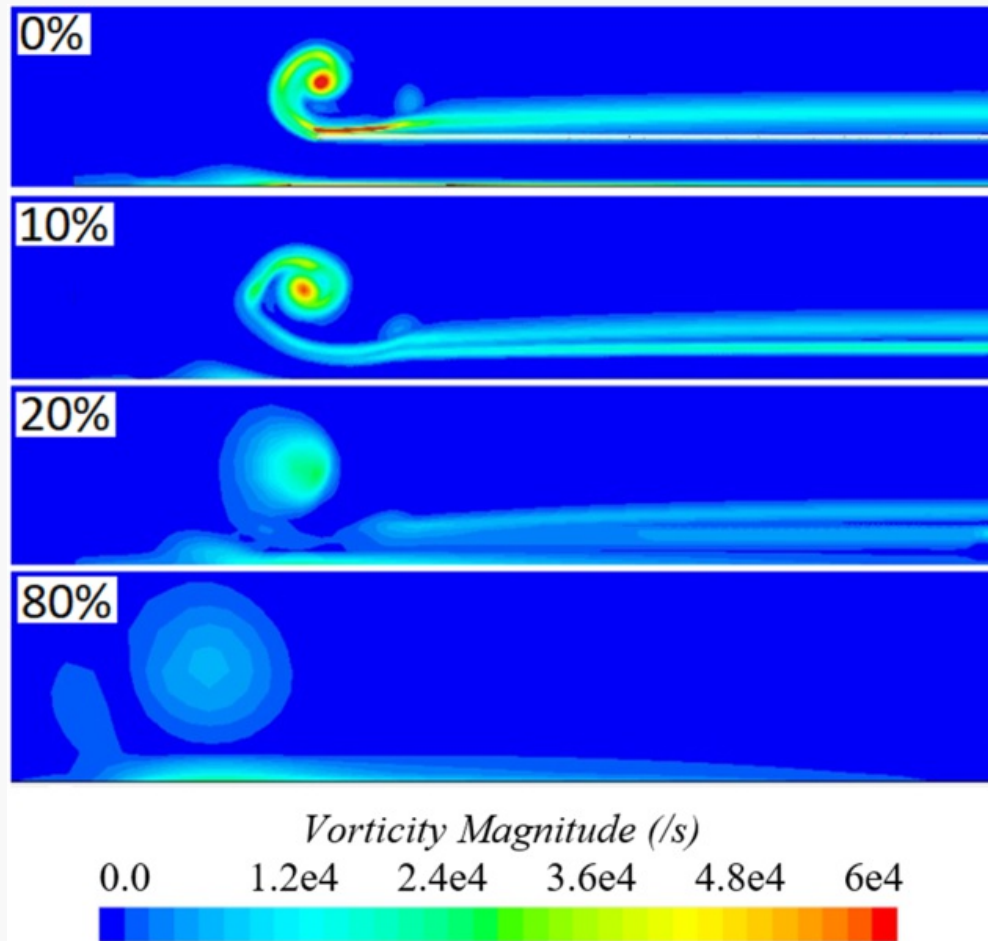
The optimized wing was compared to the base rectangular wing, with the angle of attack of the rectangular wing set to the root angle of the optimized wing as shown in Table 4. It can be seen that there is a significant increase in lift and a reduction in drag when compared to the baseline rectangular wing. Above $h/c = 0.4$ in freestream, the performance of the wing was shown to be much higher for a rearward sweep with a lower wingtip angle of attack.

Table 4 Performance gain of the optimized wing compared to the rectangular wing

h/c	Root AoA(deg)	Lift increase (%)	Drag decrease (%)	Aerodynamic efficiency increase (%)
0.05	4	18.2	28.2	41
0.1	4	12.4	26.9	36
0.2	4	8.5	24.6	31

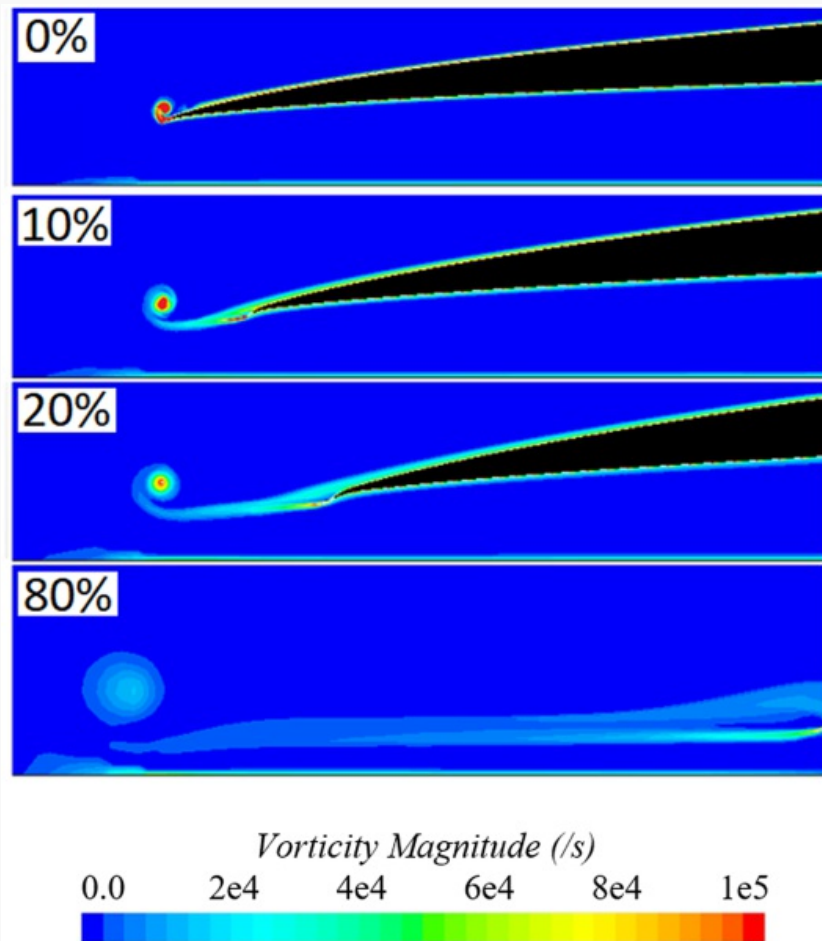
The wingtip vortex was compared between the rectangular and the optimized wing in ground effect. The rectangular wing showed a large distinctive wingtip vortex as shown in Fig. 11. This wingtip vortex moved downstream and was pushed outboard by 17% chord distance, and the vorticity of the vortex decreased downstream. The wingtip vortex induced a spanwise flow [30] which caused a turbulent boundary layer to form on the ground. The main wingtip vortex of the rectangular wing caused a separation bubble at the wingtip, which separated downstream and caused a secondary smaller counter-rotating vortex.

Fig. 11 Vorticity magnitude for rectangular wing ground effect ($h/c = 0.1$) at 0%, 10%, 20%, and 80% chord downstream



The same locations are then compared in Fig. 12 for the optimized wing. It can be seen that the vortex has a much smaller diameter, and the vorticity magnitude of the wingtip vortex is much higher than that of the rectangular wing in Fig. 11. As with the rectangular wing, the tip vortex of the optimized wing increases in diameter and the vorticity increases downstream, but the vorticity remains higher and the diameter smaller than that of the rectangular wing as the vortex travels downstream.

Fig. 12 Vorticity magnitude for the optimized wing ground effect ($h/c = 0.1$) at 0%, 10%, 20%, and 80% chord downstream



- It was seen from an optimization study of a wing in ground effect that there is no optimum wing across all ground clearances; however, a wing with a root angle of attack of 4 deg, a tip angle of attack of 6 deg, a tip chord of 20% of the root, and a forward sweep performed gave the best compromise between all cases and showed much higher performance compared to a rectangular wing.
- Tapered wings have an effectively higher aspect ratio due to the decreasing chord length along the span which increases the aerodynamic efficiency.

- Reducing tip resulted in less of the lower surface being affected by the wingtip chord due to the effective higher aspect ratio. The reduction in the tip chord from 100% to 60% resulted in a gain in lift.
- Reducing the chord along the span effectively increases the ratio h/c along the span which reduces lift seen from 60% to 13%.
- The root angle of attack had a significant effect on performance with the tip angle having minimal effect due to the forward sweep and small tip chord.

4.2 Static Trailing Edge Morphing.

Trailing edge morphing was applied to the optimized wing (shown in Fig. 10) in ground effect with a clearance of $h/c = 0.1$ by running a steady-state simulation for each morphed deflection and defined start locations shown in Table 5 with the schematic (Fig. 13) defining the root and tip start locations. Table 5 shows the corresponding start location of the morphing for each configuration applied to the optimized wing. The start location is referenced from the leading edge to the point where the morphing begins. Configurations 4 and 5 investigated variable morphed camber along the span of the wing, and this was done by investigating two morphing start locations at $0.8c$ and $0.9c$ at the root for configurations 4 and 5, respectively. The start location for the tip was located at the trailing edge of the tip which set the morphing at the wingtip to zero. This resulted in a gradual twist in the trailing edge camber which varied along the span.

Fig. 13 Wing planform schematic of morphing start locations used in Table 5

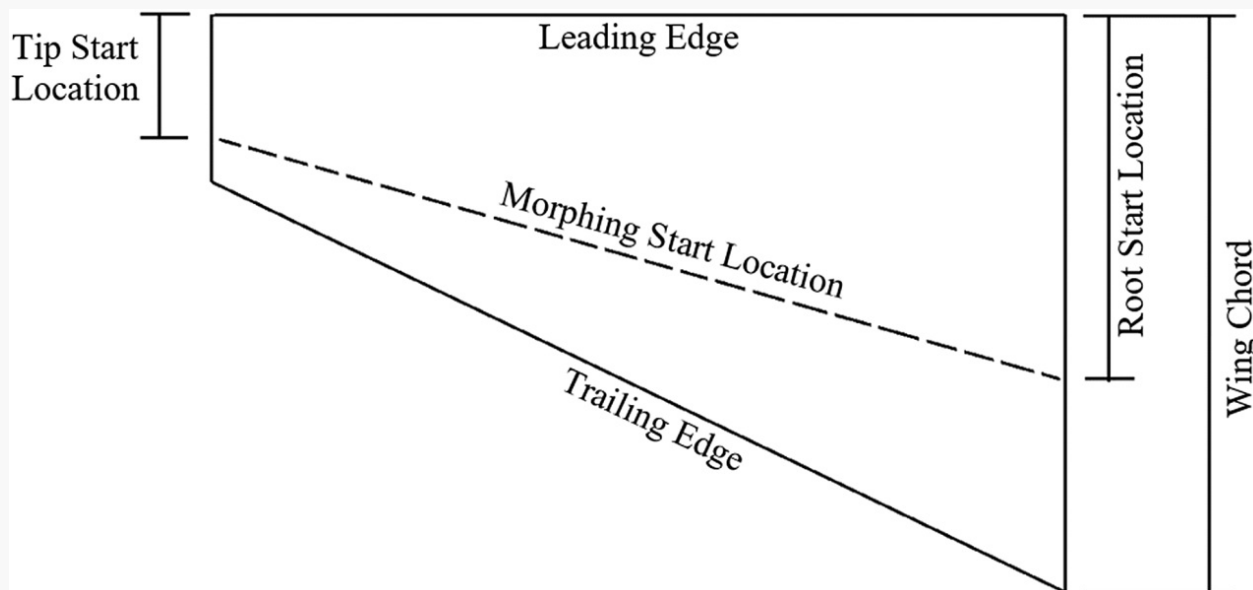


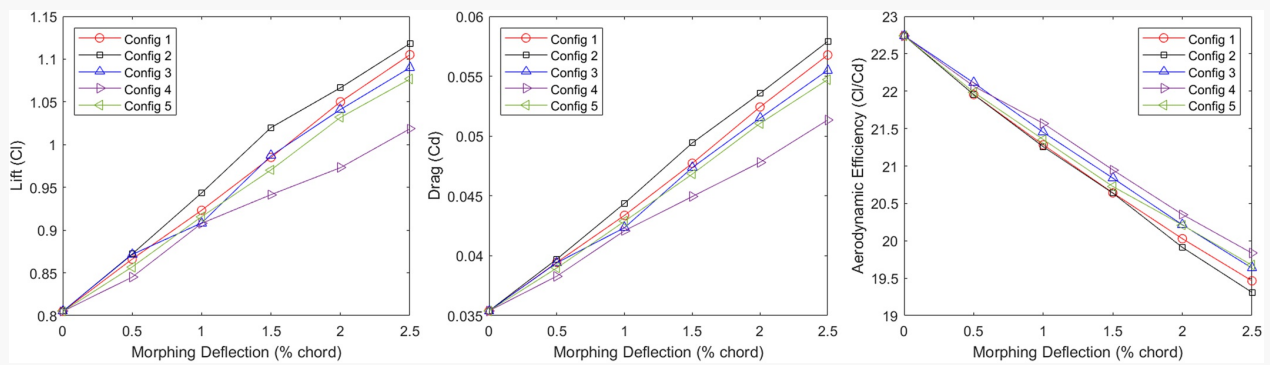
Table 5 Nondimensional morphing chord start location at root and tip

Morphing start location configuration	Tip start location	
Configuration 1	0.9c	0.10c
Configuration 2	0.9c	0.18c
Configuration 3	0.8c	0.16c
Configuration 4	0.8c	N/A
Configuration 5	0.9c	N/A

Different morphing configurations were tested on the same wing; therefore, at zero trailing edge deflection, all the configurations showed identical lift, drag, and aerodynamic efficiency. The lift seen in Fig. 14 (left) showed configuration 2 had the highest lift along with the highest drag seen in Fig. 14 (middle). Although configuration 2 had the highest drag, the rate of increase in drag was lower than the rate of increase in lift compared to the other configurations tested, resulting in the lowest aerodynamic efficiency (Fig. 14 (right)). Configuration 2 had the most aggressive morphing in terms of the curvature of the trailing edge deflection due to the later start location of the morphing along the

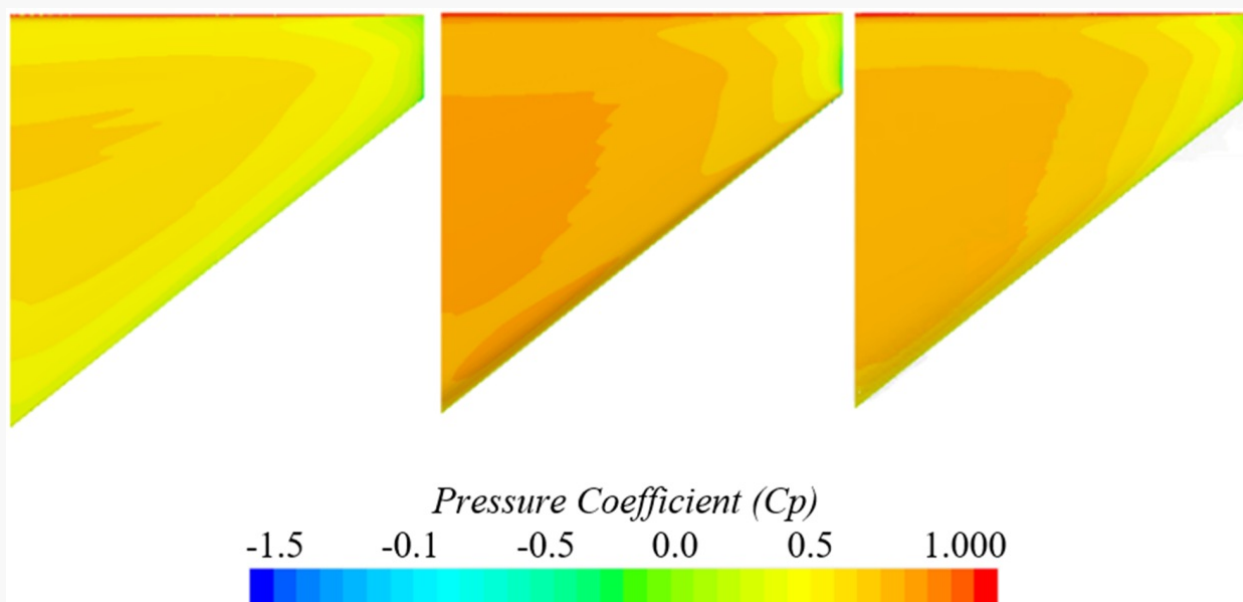
chord for both the root and tip profiles. Configuration 4 showed the lowest lift and was a C_l of 0.151 lower than configuration 2, and the drag was also lower by a C_d of 0.01. As the trailing edge was morphed, configuration 4 showed a much lower rate of gain in lift and drag compared to the other configurations tested. This resulted in a much smaller difference in lift and drag between the zero and maximum deflection compared to the other configurations. This shows that starting the morphing location at a later distance along the chord results in the highest lift and aerodynamic efficiency.

Fig. 14 Lift (left), drag (middle), and aerodynamic efficiency (right) FishBAC morphing in ground effect



Looking at the pressure on the lower surface, it can be seen that for the morphed wing (Fig. 15 middle and right) the pressure on the lower surface has increased compared to zero morphing (Fig. 15 left) corresponding to the lift seen in (Fig. 14).

Fig. 15 Lower surface pressure in ground effect ($h/c = 0.1$) for the optimized wing with zero deflection (left), 2.5% configuration 2 (middle), and 2.5% deflection configuration 4 (right)



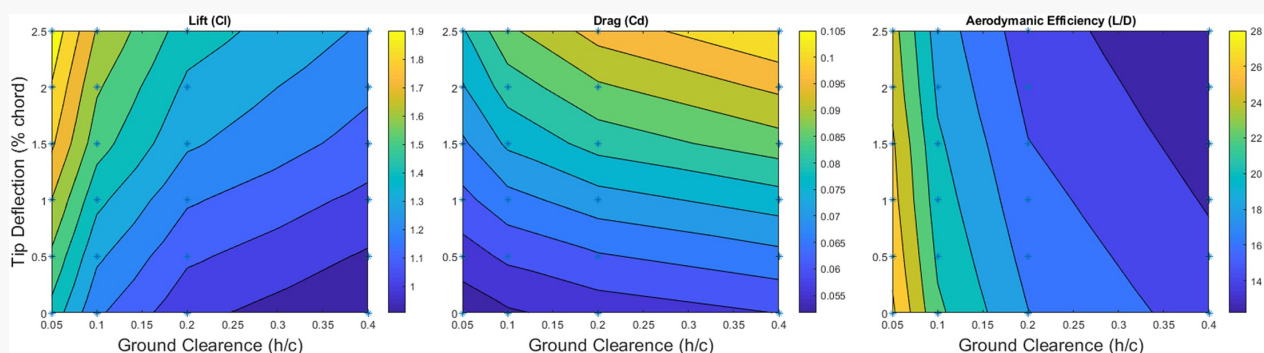
Moreover, it was seen in Fig. 15 that at the root the trailing edge pressure was the same for the different configurations tested and the zero morphing which was also seen at the midspan. This was due to the Kutta condition defining the pressure at the trailing edge causing all variations in pressure to occur upstream of the trailing edge. Comparing configuration 4 (earlier morphing start location) to configuration 2 (later morphing start location) shows a higher pressure magnitude on the lower surface for the later morphing. As the trailing edge pressure is fixed, there is a greater rate of change in pressure from the trailing edge to the point of maximum pressure on the lower surface for configuration 2. This is consistent with two-dimensional work [2] where later morphing start locations caused greater amounts of lift.

Analyzing the pressure on the wing in the spanwise direction (Fig. 15) shows that the high pressure at the root reduces toward the wingtip, with a steeper reduction in pressure nearer the wingtip. The lower pressure on the upper surface of the wing causes the wingtip vortex to form, which induces a spanwise flow on the lower surface of the wing. With the wingtip vortex core fixing the pressure at

the wingtip, the higher pressure for the later starting location caused a greater spanwise flow which fed the wingtip vortex resulting in increased drag.

Analyzing the static morphing by varying the ground clearance for configuration 2 showed that as the wing was deflected, the lift (Fig. 16 (left)), drag (Fig. 16 (middle)), and efficiency (Fig. 16 (right)) followed the same trend as $h/c = 0.1$ ground clearance. As the deflection was increased from zero to maximum, the lift increased by a significantly larger amount when in ground effect compared to $h/c = 0.4$ ground clearance, as shown in Fig. 16 (left). It was also seen that the drag increased a greater amount at $h/c = 0.4$ ground clearance when the airfoil was morphed Fig. 16 (middle). Figure 16 (right) shows that varying the ground clearance had a significantly larger effect on the aerodynamic efficiency compared to morphing the trailing edge. This was due to the fact that reducing the ground clearance which increased the lift and reduced the induced drag, whereas increasing the trailing edge deflection increased both the lift and drag. As the aerodynamic efficiency is defined by the ratio of lift to drag, the increase in lift and the decrease in drag had a much larger effect on the aerodynamic efficiency. Varying the ground clearance from $h/c = 0.4$ to $h/c = 0.05$ resulted in a 14% reduction in aerodynamic efficiency compared to morphing the trailing edge from 0% to 2.5%, which reduced aerodynamic efficiency by 2% at $h/c = 0.4$ and approximately 4% at $h/c = 0.5$:

Fig. 16 Configuration 2 lift (left), drag (middle), and aerodynamic efficiency (right)



- The location along the chord at which the morphing began had a large effect on the wing performance, with a later start location resulting in higher lift and drag and lower aerodynamic

efficiency.

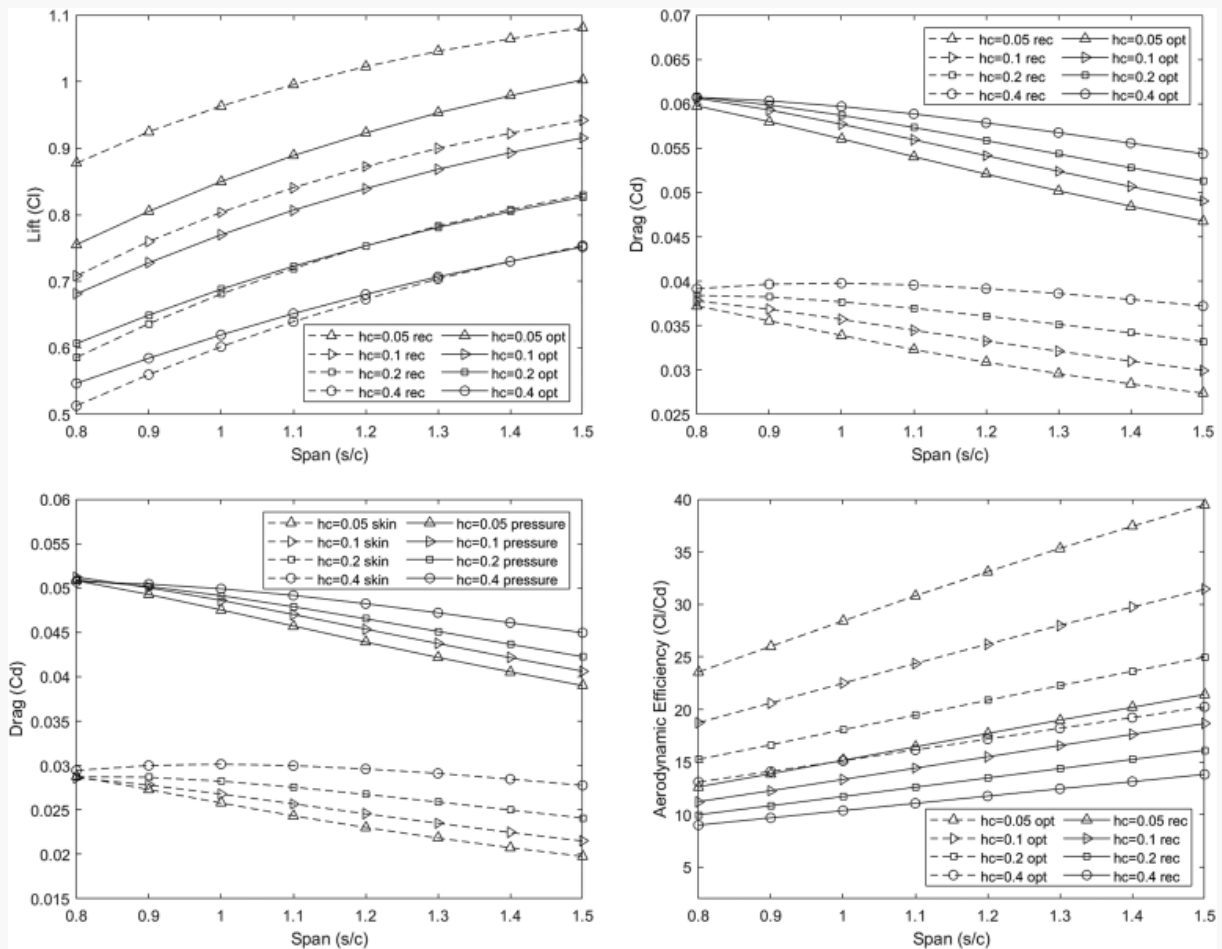
- A later start location caused greater volume beneath the wing, which increased the pressure on the lower surface.
- The Kutta condition fixed the trailing edge pressure which caused the lower surface pressure to increase as the camber was morphed.

4.3 Extending Span Morphing.

It was found that reducing the tip chord effectively increased the aspect ratio of the wing which improved the wing performance. This was further investigated by taking the optimized wing and morphing the wing in the spanwise direction to increase the wingspan. Wings in ground effect vehicles tend to have low aspect ratio wings, as rolling of the craft in ground effect can cause a wingtip to touch the surface and cause the craft to crash. However, there are instances where the craft is not rolling, such as cursing, which is the focus of the span-extending morphing in this study to improve the wing performance.

As seen in the previous sections (4.1-4.3), [AQ6](#) reducing the ground clearance increased the lift (Fig. 17 top left) and reduced the drag (Fig. 17 top right), which improved the overall aerodynamic efficiency (Fig. 17 bottom right) as the wing was brought into ground effect, and this was seen for all span lengths. For the optimized wing, the variation in lift was much greater between the different ground heights. For $h/c = 0.2$ and 0.4 , between a span of 1 and 1.5, there is no difference in lift (Fig. 17 top left) when comparing the rectangular and optimized wings; however, the total drag (Fig. 17 top right) shows a significant difference which improved the overall aerodynamic efficiency. This shows that the drag was affected at much larger ground clearances compared to the lift when analyzing the rectangular and optimized wing. At lower ground clearances below $h/c = 0.2$, there was a significant difference in lift and drag reduction, which means that both the lift increase and drag reduction contribute to the increase in aerodynamic efficiency. It was found that as the ground clearance of the optimized wing decreased, the drag decreased at a greater rate, but the lift increased at a greater rate below $h/c = 0.2$. By comparing the rectangular and optimized wings in this section, it was seen that by varying the aspect ratio, the optimized wing still showed superior performance to the rectangular wing.

Fig. 17 Span morphing lift (top left), drag (top right), and aerodynamic efficiency (bottom right) for rectangular and optimized NACA6409 wing, and drag components (bottom left) for the optimized wing

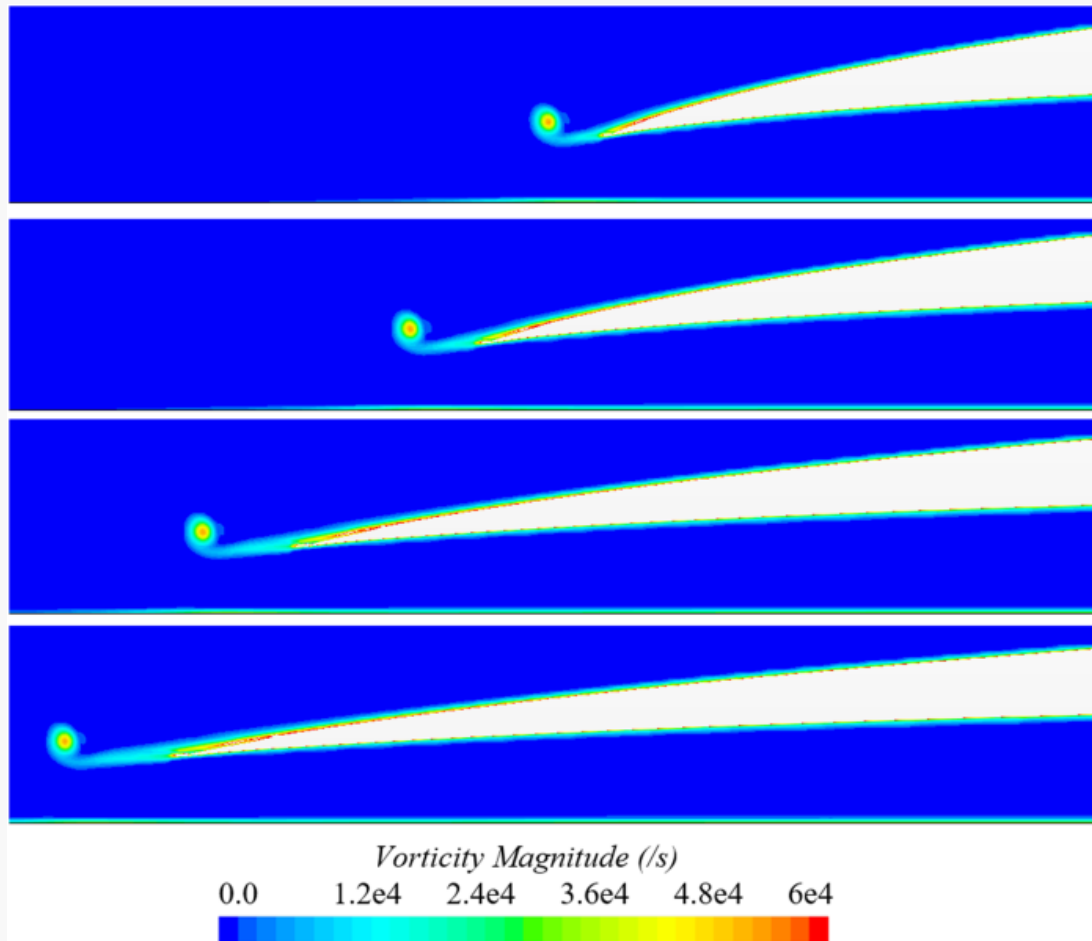


There are two types of drag known as skin friction drag and pressure drag, and their sum gives the total drag. Morphing the span of the wing increases the total surface area, and as both the pressure and skin friction drag are proportional to the surface area, a breakdown of these drags has been shown in Fig. 17 (bottom right). It can clearly be seen that the pressure drag is more dominant than the skin friction drag, and that the pressure drag was significantly affected by the variation in ground clearance and span opposed. The pressure drag was seen to vary much more when the ground clearance was varied for a larger span.

Increasing the half-span length of the wing from 80% to 150% of the chord length showed a reduction in total drag. At 40% ground clearance, the pressure drag initially increased as the half span increased to 100% of the chord and then decreased as the span was increased from 100% to 150%. The initial increase was due to the increase in lift causing a larger wingtip vortex which increased the induced drag. Increasing the span beyond 100% does not increase the vortex any further; therefore, increasing the span reduces the effect of the wingtip vortex on the wing surface pressure. When analyzing the surface pressure coefficient, the pressure on the upper surface had minimal change with the span morphing. However, the lower surface shows significant pressure variations. The pressure on the lower surface is reduced due to the span-induced flow feeding the wingtip vortex. This distance where the flow was affected remained a constant length between 130% and 150%, showing that wings with a higher aspect ratio are less affected by the wingtip vortex. The root of the wing at 150% span shows significantly larger pressure values which extends over a greater proportion of the lower surface. This explains the large increase in lift with increasing span.

The vorticity of the wingtip vortex was also analyzed, and it was found that increasing the span had minimal impact on the wingtip vortex. Both the vorticity and the vortex diameter remained constant as the span increased which showed why the aerodynamic efficiency increased with the larger aspect ratio wing due to the reduced amount of induced drag. Although this can be seen in Fig. 18 at a location of 30% chord behind the wing, the wingtip vortex was analyzed at different plane locations and showed the same behavior.

Fig. 18 NACA6409 at 4 deg AoA in 10% ground effect at 80% (top), 100%, 130%, and 150% (lower) span showing vorticity at 30% of the root chord from leading edge



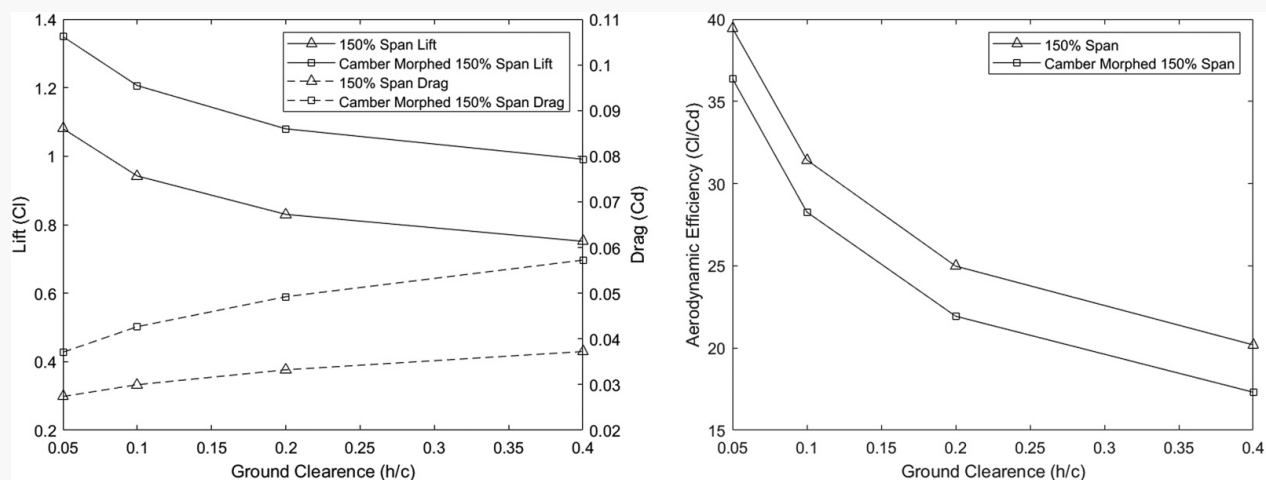
- Low aspect ratio wings allow the craft to roll without a wingtip touching the ground; however, high aspect ratio wings increase aerodynamic performance.
- For cruising, the span was increased by 150%, resulting in an increase in lift and aerodynamic efficiency and a reduction in drag.
- Increasing the span reduced the impact of the wingtip vortex on the wing, resulting in a higher overall pressure on the lower surface.

4.4 Extending Span and Camber Combination.

In this study, extending the span of a wing in ground effect has been shown to increase the aerodynamic performance for cruise conditions while allowing a smaller span for the craft to roll without a wing touching the ground. Camber morphing was also applied to the wing which has the potential to further improve performance, as camber morphing requires smaller deflections for the same amount of roll rate compared to traditional control surfaces [31]. Camber morphing is also a continuous surface that improves aerodynamic efficiency as traditional control surfaces typically have a gap between the flap and the wing, which reduces aerodynamic efficiency. This section looks at the combination of both the span and camber morphing to create the optimized wing.

A morphed deflection of 2% trailing edge with a start location of $0.9c$ at the root and $0.1c$ at the tip was carried out for ground clearance between $h/c = 0.05$ and 0.4 . Comparisons were made between a nonmorphed and morphed 150% span wing. Comparing the lift (Fig. 19 left) shows for both cases and previously seen that reducing the ground clearance increased the lift and reduced the drag of the wing. [AQ7](#) It was also seen that the lift was higher for the camber morphed wing which is consistent with the smaller span seen in Sec. 4.2. It was also seen that the efficiency (Fig. 19 rightleft) decreased as the trailing edge deflection increased as a result of the large drag gains from the camber morphing. As seen in the smaller span case in Sec. 4.2, the rate of increase in lift and drag increases as the wing becomes closer to the ground due to the increase in ground effect enhancement. Overall, it is seen by morphing the optimized wing trailing edge by 2% of the root chord that the lift is increased by 20% in small ground clearances and by 25% at higher ground clearances. The drag (Fig. 19 left) increased by 26% at small ground clearances and by 35% at larger ground clearances. The reason for the large reductions in drag at higher ground clearances was due to the smaller blockage effect beneath the wing.

Fig. 19 Optimized 150% span wing with and without camber morphing lift and drag (left) and aerodynamic efficiency (right)



- Camber morphing shows the same characteristics with the extended span compared to a smaller span.
- Lift and drag increased as the trailing edge deflection increased due to the decreasing gap between the trailing edge and ground resulting in lower aerodynamic efficiency.

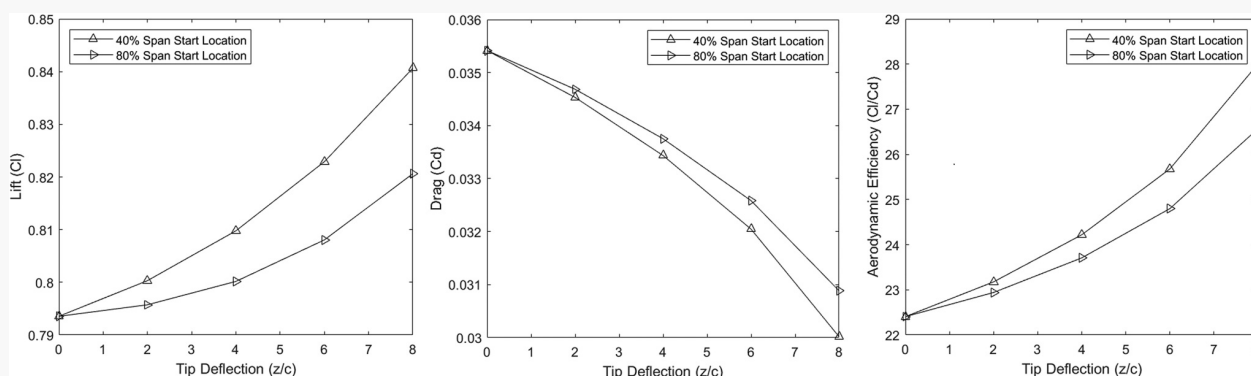
4.5 Wingtip Morphing.

In this study, it was clear that the wingtip vortex had a large impact on the wing performance especially on the wing lower surface pressure. The effect of the wingtip vortex was seen to be reduced by increasing the wing aspect ratio using extendable wings; however, the wingtip can be morphed downwards to seal the lower surface during cruise and then morphed upwards to allow the craft to roll without touching the ground surface. A similar study was carried out by Wei and Zhigang [9] who investigated effectively hinged wingtips, and this study extends this research by applying the FishBAC morphing previously seen applied in the chord direction and applying it to the span direction.

When applying the FishBAC morphing in the span direction, the morphing start locations were tested at both 40% and 80% from the root along the span. Keeping the root at a fixed ground

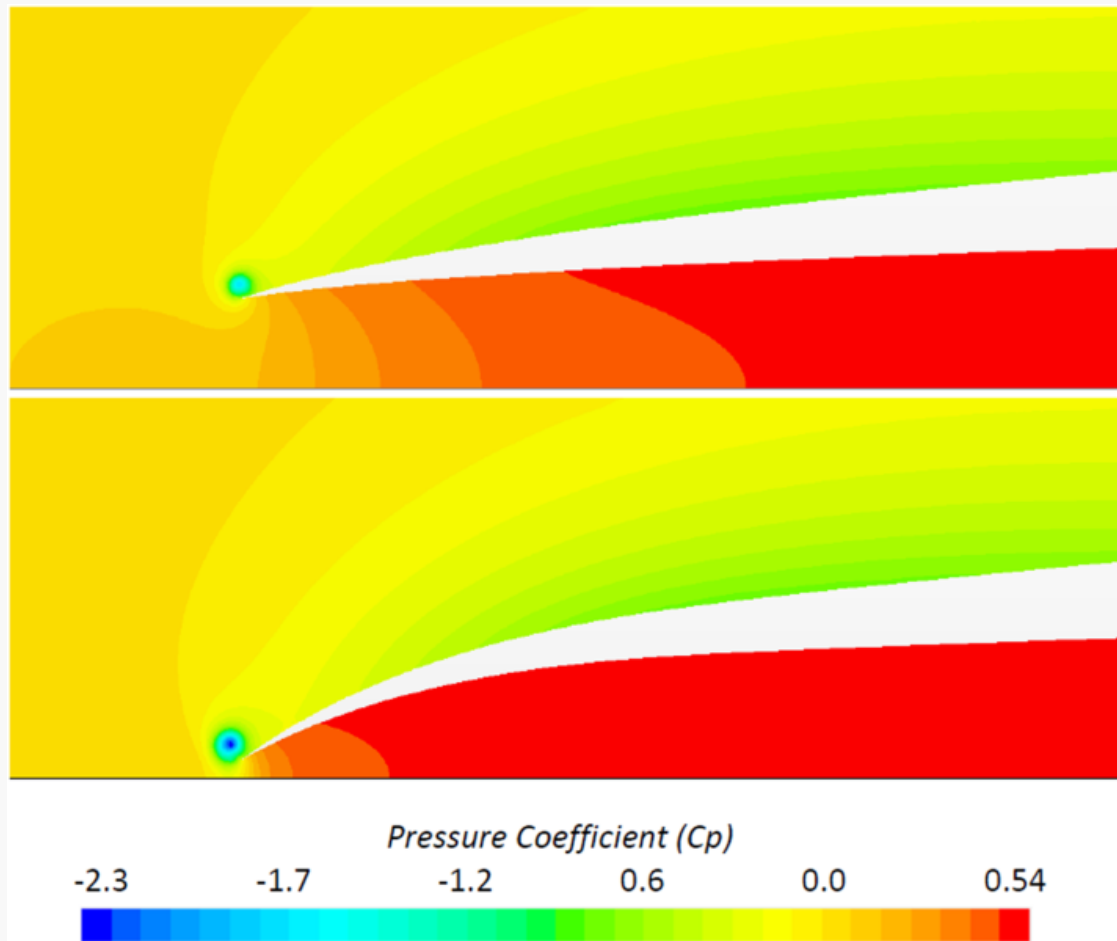
clearance of $h/c = 0.1$, the wingtip was morphed downwards. This had a large impact on the performance of the wing causing the lift and aerodynamic efficiency to increase as shown in Fig. 20 and showing similar trends to the hinged wingtip of Wei and Zhigang [9].

Fig. 20 Lift (left), drag (middle), and aerodynamic efficiency (right) of FishBAC morphing wingtip in ground effect



The gain in performance can be best described by looking at the pressure contours (Fig. 21) of the wing on a plane at a location 20% of the chord downstream of the leading edge. Looking first at the unmorphed wing, it was seen the lower surface pressure began to reduce approximately midspan showing that the flow is highly three-dimensional. Morphing the wingtip to a clearance of 2% chord shows that the high pressure now extends almost the full span. This is due to the restrictive gap between the wingtip and ground when morphed, effectively sealing the lower. It can also be seen that the wingtip vortex was pulled downwards when the tip was morphed, and also that the wingtip vortex had a lower core pressure when in ground effect.

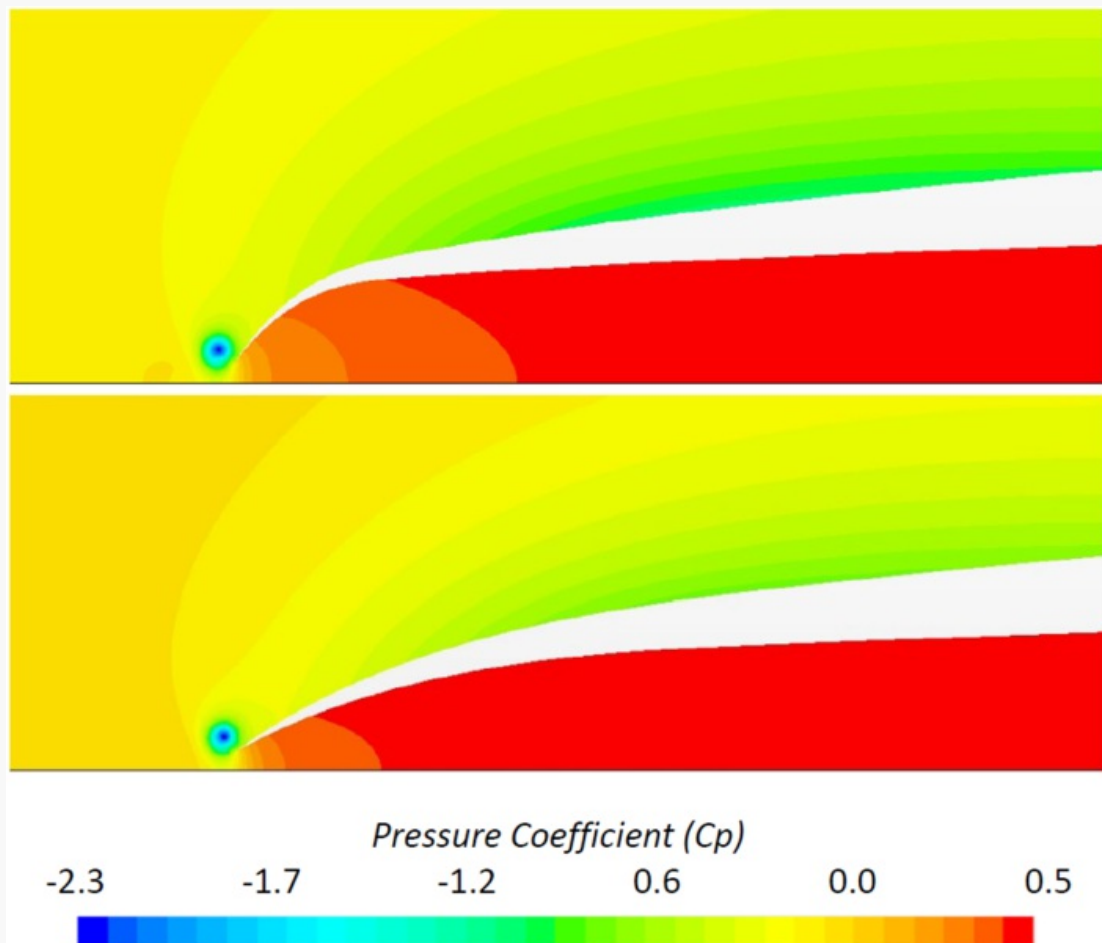
Fig. 21 Pressure coefficient of the wing at 20% downstream from the leading edge for zero morphing (upper) and maximum deflection starting at 40% (lower)



In the lift, drag, and aerodynamic efficiency plots, it was seen that there was a large variation between the 40% and 80% morphing start locations. Comparing the pressure on a plane behind the wing at 20% chord from the leading edge showed Fig. 22 a higher pressure for a greater distance along the span beneath the wing. This was due to the earlier start location resulting in the wing becoming lower to the ground as the wingtip was morphed effectively reducing the ground clearance and further enhancing the ground effect. The earlier the start position, the higher the lift and aerodynamic efficiency, and the lower the drag. This was due to the camber morphing where a later

start position had higher performance, and this was due to the camber morphing having a fixed trailing edge pressure from the Kutta condition unlike the wingtip when considering the flow in the spanwise direction.

Fig. 22 Pressure coefficient on plane 20%c from the leading edge for 80% (upper) and 40% (lower) span start locations at maximum deflection



- Using the FishBAC method of morphing in the spanwise direction, the wingtip was morphed downwards, increasing lift and aerodynamic efficiency and reducing drag compared to a nonmorphed wingtip.
- Morphing the wingtip allows the craft to cruise at a much higher aerodynamic efficiency, while

still allowing the wingtip to rise to allow the craft to roll.

- Morphing the wingtip pulls the wingtip vortex downwards and seals the wing lower surface which increases the pressure beneath the wing.
- Morphing the wingtip results in a minimal pressure drop at the wingtip in the span direction compared to a nonmorphing wing where the tip vortex affects the pressure from the midspan.

5 Conclusion

An optimization study was carried out first on a three-dimensional NACA6409 wing with an aspect ratio of 2, focusing on the application of span and trailing edge morphing in ground effect flight. Optimization was carried out on the rectangular wing, by varying the tip and root angle of attack, tip chord, and tip position. The root and tip angle of attack were varied independently to vary the twist of the wing. The optimization was carried out in star ccm+ Design Manager using steady-state simulation for each design and a Reynolds-averaged Navier–Stokes solver with the k -Omega turbulence model.

With an emphasis on improving aerodynamic efficiency, the optimization study focused on maximizing lift and reducing drag. From the analysis of the output designs, a wingtip chord of 20% was identified as having the best aerodynamic performance. This was due to the smaller tip chord effectively increasing the aspect ratio of the wing. A forward sweep showed the best aerodynamic performance due to a rearward sweep feeding the wingtip vortex which increased drag. The root angle of attack increased the pressure on the lower surface which increased the spanwise flow feeding the wingtip vortex and thus increasing drag. Therefore, a low angle of attack at the root produced the highest aerodynamic efficiency. In contrast to this, the wingtip angle of attack for a 20% chord had little effect on the aerodynamic efficiency. From the Pareto, two designs were selected as optimum designs both with a 20% tip chord and a wingtip trailing edge of 80% of the root chord upstream of the root trailing edge. The design with a 2-deg root and 8-deg wingtip was identified as a high-efficiency design and the 4-deg root and 6-deg tip as a lower efficiency but with high lift. Both these designs showed an increase in efficiency of up to 41% in extreme ground effect and up to 31% at 20% ground clearance when compared to the original rectangular wing. This increase was due to a reduction in drag and an increase in lift compared to the rectangular wing.

Trailing edge morphing was then applied to the optimized wing in ground effect. Five different start locations were tested, and these combinations varied both the root and tip start locations. It was seen that the lowest lift during morphing was achieved by starting the morphing at 80% on the root chord and no morphing at the tip, resulting in a twisted morphing trailing edge. The highest lift was obtained by starting the morphing at 90% on the root chord and 18% from the leading edge on the tip chord, with all percentages with respect to the root chord. The later morphing resulted in the highest lift due to the pressure being fixed at the trailing edge throughout the morphing, so the later morphing causes the pressure to increase rapidly and therefore an overall higher pressure on the lower surface. It was found that the highest lift configuration of the morphing start location also had the highest drag, resulting in the lowest aerodynamic efficiency. Therefore, configuration 2 with a start location of 0.9c at the root and 0.18c at the tip had the lowest efficiency, and configuration 4 with a start location of 0.8c root had the highest efficiency. The increase in drag was caused by the higher pressure beneath the wing for the higher lift configuration feeding the wingtip vortex which increases the drag. Also, the drag increased due to the higher blockage beneath the wing.

Span morphing, which increases the aspect ratio of the wing, was also investigated. Increasing the span from 1c to 1.5c increased the lift by 15.1% and the aerodynamic efficiency by 27.4% in at $h/c = 0.1$ ground effect. This is due to the wingtip vortex remaining constant in size and strength as the span increases and therefore has less of an influence on the wing at higher aspect ratios. Increasing the ground clearance reduced the gains in lift and aerodynamic efficiency from the span morphing, and reducing the ground clearance increased the gains in lift and aerodynamic efficiency. Wings in ground effect vehicles typically have low aspect ratios to allow the craft to roll without a tip touching the surface; therefore, span morphing would ideally be suited to cruising or to the higher lift wing of the craft when turning by rolling the craft. The camber morphing was also applied to the 150% span, where it was seen that the aerodynamic characteristics were very similar for both 100% and 150% spans.

The wingtip was morphed using the FishBAC method applied in the span direction where significant gains in performance could be achieved. Morphing the wingtip increased the lift and aerodynamic efficiency compared to a nonmorphed wingtip and reduced drag. Two different morphing start

locations were carried out at 40% and 80% from the root chord. It was found that the earlier start location produced the highest performance gains, as it brought the trailing edge closest to the ground, causing further enhancements in ground effect. This increased lift and aerodynamic efficiency as well as reduced the drag. This was in contrast to the camber morphing where a later start location caused higher performance; however, the wingtip was not maintained by the Kutta condition like the trailing edge.

This paper has focused on finding an optimal wing for a WIG craft. Although this paper focuses on applying span and trailing edge morphing to the optimized wing, further research could be applied to modify the shape of the wing to ensure that the wing remains on the Pareto front for all ground clearances.

Acknowledgment

The authors acknowledge the use of the IRIDIS High Performance Computing Facility, and associated support services at the University of Southampton, in the completion of this work.

Funding Data

- Engineering and Physical Sciences Research Council (2218985; Funder ID: 10.13039/501100000266).

Data Availability Statement

The datasets generated and supporting the findings of this article are obtainable from the corresponding author upon reasonable request.

Nomenclature

$A =$ wing area

$AR =$ aspect ratio

$B =$

	wingspan
$c =$	root chord length
$C_d =$	drag coefficient
$C_l =$	lift coefficient
$D =$	drag
$dlc =$	wingtip height (dihedral)
$GE =$	ground effect
$h/c =$	ground clearance to chord ratio
$L =$	lift
$ld =$	aerodynamic efficiency
$lc =$	sweep distance
$TE =$	trailing edge
$TKE =$	turbulent kinetic energy
$u =$	velocity
$X =$	distance along airfoil
$X_s =$	morphing start location
$yc =$...

trailing edge deflection to chord ratio

$Y_t =$
airfoil thickness

$\theta_r =$
root angle of attack


$\theta_t =$
tip angle of attack


References


- [1] Rozhdestvensky, K. V., 2006, "Wing-in-Ground Effect Vehicles," *Prog. Aerosp. Sci.*, 42(3), pp. 211–283. [10.1016/j.paerosci.2006.10.001](https://doi.org/10.1016/j.paerosci.2006.10.001) 
- [2] Clements, D., and Djidjeli, K., 2023, "Aerodynamic Performance of Morphing and Periodic Trailing-Edge Morphing Airfoils in Ground Effect," *J. Aerosp. Eng.*, 36(3), p. 4023012. [10.1061/JAEEZZ.ASENG-4707](https://doi.org/10.1061/JAEEZZ.ASENG-4707) 
- [3] Qu, Q., Jia, X., Wang, W., Liu, P., and Agarwal, R. K., 2014, "Numerical Study of the Aerodynamics of a NACA 4412 Airfoil in Dynamic Ground Effect," *Aerosp. Sci. Technol.*, 38, pp. 56–63. [10.1016/j.ast.2014.07.016](https://doi.org/10.1016/j.ast.2014.07.016) 
- [4] Abramowski, T., 2007, "Numerical Investigation of Airfoil in Ground Proximity," *J. Theor. Appl. Mech.*, 45(2-), pp. 425–436. URL = www.ptmmts.org. [AQ13](#) 
- [5] Ahmed, M. R., and Sharma, S. D., 2005, "An Investigation on the Aerodynamics of a Symmetrical Airfoil in Ground Effect," *Exp. Therm. Fluid Sci.*, 29(6), pp. 633–647. [10.1016/j.expthermflusci.2004.09.001](https://doi.org/10.1016/j.expthermflusci.2004.09.001) 
- [6] Jung, K. H., Chunn, H. H., Kim, H. J., Chun, H. H., and Kim, H. J., 2008, "Experimental Investigation of Wing-in-Ground Effect With a NACA6409 Section," *J. Mar. Sci. Technol.*, 13(4), pp. 317–327. [10.1007/s00773-008-0015-4](https://doi.org/10.1007/s00773-008-0015-4) 
- [7] Lee, J., Han, C. S., and Bae, C. H., 2010, "Influence of Wing Configurations on Aerodynamic Characteristics of Wings in Ground Effect," *J. Aircr.*, 47(3), pp. 1030–1040. [10.2514/1.46703](https://doi.org/10.2514/1.46703) 


- [8] Lu, A., Tremblay-Dionne, V., and Lee, T., 2019, "Experimental Study of Aerodynamics and Wingtip Vortex of a Rectangular Wing in Flat Ground Effect," *ASME J. Fluids Eng.*, 141(11), p. 111108.10.1115/1.4043593 
- [9] Wei, Y., and Zhigang, Y., 2012, "Aerodynamic Investigation on Tilttable Endplate for WIG Craft," *Aircr. Eng. Aerosp. Technol.*, 84(1), pp. 4–12.10.1108/00022661211194933 
- [10] Niroomi, M., 2018, "Aerodynamic and Static Stability Characteristics of Airfoils in Extreme Ground Effect," *Proc. Inst. Mech. Eng., Part G: J. Aerosp. Eng.*, 232(6), pp. 1134–1148.10.1177/0954410017708212 
- [11] Qu, Q., Wang, W., Liu, P., and Agarwal, R. K., 2015, "Airfoil Aerodynamics in Ground Effect for Wide Range of Angles of Attack," *AIAA J.*, 53(4), pp. 1048–1061.10.2514/1.J053366 
- [12] Yun, L., Bliault, A., and Doo, J., 2010, *WIG Craft and Ekranoplan: Ground Effect Craft Technology*, Springer, New York. 
- [13] Park, K., Hong, C. H., Kim, K. S., and Lee, J., 2008, "Effect of Endplate Shape on Performance and Stability of Wings-in-Ground (WIG) Craft," *World Acad. Sci., Eng. Technol.*, 2(11), pp. 296–302. url={https://api.semanticscholar.org/CorpusID:1415077} 
- [14] Flaig, J., 2019, "A Different Kettle of Fish: Is Airfish 8 Plane-Boat Hybrid a Marine Travel Game-Changer?," <https://www.imeche.org/news/news-article/a-different-kettle-of-fish-is-airfish-8-plane-boat-hybrid-a-marine-travel-game-changer>, accessed Feb 2023. [AQ8](#) 
- [15] Bashir, M., Lee, C. F., and Rajendran, P., 2017, "Shape Memory Materials and Their Applications in Aircraft Morphing: An Introspective Study," *ARPN J. Eng. Appl. Sci.*, 12(19), pp. 5434–5446. url={https://api.semanticscholar.org/CorpusID:210915583} 
- [16] Alsaidi, B., Joe, W. Y., and Akbar, M., 2019, "Computational Analysis of 3D Lattice Structures for Skin in Real-Scale Camber Morphing Aircraft," *Aerospace*, 6(7), p. 79.10.3390/aerospace6070079 


- [17] Frommer, J., and Crossley, W., 2005, "Enabling Continuous Optimization for Sizing Morphing Aircraft Concepts," AIAA Paper No. 2005-816. [10.2514/6.2005-816](#) 
- [18] Beaverstock, C. S., Woods, B. K. S., Fincham, J. H. S. M., and Friswell, M. I., 2015, "Performance Comparison Between Optimised Camber and Span for a Morphing Wing," *Aerospace*, 2(3), pp. 524–554. [10.3390/aerospace2030524](#) 
- [19] Ajaj, R. M., Friswell, M. I., Saavedra Flores, E. I., Little, O., and Isikveren, A. T., 2012, "Span Morphing: A Conceptual Design Study," AIAA Paper No. 2012-1510. [10.2514/6.2012-1510](#) 
- [20] Yu, Y., Liu, Y., and Leng, J., 2009, "Design and Aerodynamic Characteristics of a Span Morphing Wing," *Proc. SPIE*, 7290(-U), p. 72900U. <https://doi.org/10.1016/j.ast.2023.108721> 
- [21] Jung, J. H., Kim, M. J., Yoon, H. S., Hung, P. A., Chun, H. H., and Park, D. W., 2012, "Endplate Effect on Aerodynamic Characteristics of Three-Dimensional Wings in Close Free Surface Proximity," *Int. J. Nav. Archit. Ocean Eng.*, 4(4), pp. 477–487. [10.2478/IJNAOE-2013-0112](#) 
- [22] Macaraeg, M., 1998, "Fundamental Investigations of Airframe Noise," AIAA Paper No. 98-2224. [10.2514/6.98-2224](#) 
- [23] Jeong, J., and Bae, J. S., 2022, "Wind Tunnel Flight Test of VCCS Morphing UAV," 2022 International Conference on Unmanned Aircraft Systems (ICUAS 2022),  Dubrovnik, Croatia, 2022, doi: [10.1109/ICUAS54217.2022.9836192](#), pp. 1424–1431. [AQ9](#) 
- [24] Woods, B. K. S., and Friswell, M. I., 2012, "Preliminary Investigation of a Fishbone Active Camber Concept," ASME Paper No. SMASIS2012-8058. [10.1115/SMASIS2012-8058](#) 
- [25] Siemens Digital Industries Software, 2019, User Manual Star CCM+ 14.04.013,  [AQ10](#) 
- [26] Coleman, H., and Members, C., 2009, "Standard for Verification and Validation in Computational Fluid Dynamics and Heat Transfer (V&V20 Committee Chair and Principal Author),"


ASME, \ast , Standard No. ASME V&V 20-2009, University of Alabama, Huntsville. [AQ11](#) 

[27] Yang, Z.-G., Yang, W., and Jia, Q., 2010, "Ground Viscous Effect on Stall of Wing in Ground Effect," Eng. Appl. Comput. Fluid Mech., 4(4), pp. 521–531 [please change this citation to "Ying Chengjiong, Yang Wei and Yang Zhigang, Ground Viscous Effect on Stall of Wing in Ground Effect, 2010, The Third International Conference on Modelling and Simulation (ICMS2010), ISBN 978-1-84626-153-4, Wuxi, P.R.China, June. 4-6, 2010, pp.230-233" as my citaion software export the wrong names to the file.] 


[28] Mohamed, M., and Amin, I., 20162020 [date should be 2020], "Effect of Wing Geometrical Parameters on the Aerodynamic Performance of Wing in Ground Marine Craft," Proceedings of Third International Conference on Maritime Technology and Engineering (MARTECH 2016), Vol. 1, \ast , London, ISBN 978-1-138-03000-8, pp. 347–352. 


[29] Fink, M. P., and Lastinger, J. L., 1986, "Aerodynamic Characteristics of Low-Aspect-Ratio Wings in Close Proximity to the Ground," Biol. Cent.-Am., 2(\ast), [url={https://api.semanticscholar.org/CorpusID:110018913}] pp. v–413. 


[30] Harvey, J. K., and Perry, F., 1971, "Flowfield Produced by Trailing Vortices in the Vicinity of the Ground," AIAA Journal, Volume 9, Issue 8, \ast , \ast , pp. 1659–1660. [AQ12](#) 


[31] Abdessemed, C., Bouferrouk, A., and Yao, Y., 2022, "Effects of an Unsteady Morphing Wing With Seamless Side-Edge Transition on Aerodynamic Performance," Energies, 15(3), p. 1093.10.3390/en15031093 


Author Query


1. **Query [AQ1]** : Please provide postal code for affiliations. Also check and confirm the edits made in affiliations. 

Response by Author: "Have added postcode as a comment. SO16 7QF"
2. **Query [AQ2]** : Please define EMC, WIG, and AoA at first occurrence. 


Response by Author: "Have removed EMC as not needed and have defined AoA and WIG when first appeared in the introduction. Many thanks"
3. **Query [AQ3]** : We have reworded the sentence beginning "A value of 0.9944 for the..." for clarity. Please check that your meaning is preserved. 

Response by Author: "Many thanks, have added the word convergence "
4. **Query [AQ4]** : In the sentence beginning "An optimization study was carried out using the..." Please specify which table "Table ??" refers to here. 

Response by Author: "Sorry this should not be a table, this should say figure 2. "
5. **Query [AQ5]** : Figures must be cited in numerical order. Please check renumbering of Figs. 7 and 8. 

Response by Author: "Accepted"
6. **Query [AQ6]** : In the sentence beginning "As seen in the previous..." Please specify which section "in the previous sections" refers to here. 


Response by Author: "sections (4.1-4.3)"

7. **Query [AQ7]** : Figures 19 and 21 were not cited in text. Please check their insertions. 


Response by Author: "Have added in a couple more to cite efficiency and drag"

8. **Query [AQ8]** : Please provide complete details for Ref. 14. 

Response by Author: "have added to the reference, please check this is ok, thank you"

9. **Query [AQ9]** : Please provide proceeding held location (city and state/country) and date for Refs. 23 and 28. 


Response by Author: "Added these"

10. **Query [AQ10]** : Please provide author group, publisher name, and location (city and state/country) for Ref. 25. 


Response by Author: "Have cited accoring to <https://community.sw.siemens.com/s/question/0D54O000075Nz8xSAC/how-do-i-cite-simcenter-starccm> which is the software manufacture who do not provide a location but do have several headquarters/locations around the world."

11. **Query [AQ11]** : Please provide location (city and state/country) for Ref. 26. 


Response by Author: "Answered within text"


12. **Query [AQ12]** : Please provide journal title and volume number for Ref. 30. 


Response by Author: "Answered within text"

13. **Query [AQ13]** : Please provide DOI/URL for the Refs. 4, 13, 15, 20, 27, and 29. 
Response by Author: "Answered within text"

General Query

1. **Query [GQ1]** : Reminder - the ASME Copyright Agreement that was signed by all authors includes the following: "You have the right to enter into this Copyright Form and to make the assignment of rights to ASME. If the Paper contains excerpts from other copyrighted material (including without limitation any diagrams, photographs, figures or text), you have acquired in writing all necessary rights from third parties to include those materials in the Paper, and have provided appropriate credit for that third-party material in footnotes or in a bibliography." As required, ASME may contact the authors to obtain a copy of the written permission.
Response by Author: "Ok" 

2. **Query [GQ2]** : Any content obtained from the web and included in the paper may require written permission and appropriate credit if it is copyrighted content. If copyright status cannot be determined, this content should not be included in the paper
Response by Author: "Ok" 

3. **Query [GQ3]** : Please note the figures in this proof are low resolution, the final paper will publish with all figures as 300 dpi.
Response by Author: "Ok" 


4. **Query [GQ4]** : This is a reminder that your graphical abstract figure must be a 

figure from your approved final manuscript. Failure to adhere to this requirement will result in your article being placed on hold until the correct artwork is supplied.

Response by Author: "Ok"

Comments

1.

Comment by Author: "Please add in post code SO16 7QF" 

[AUTHOR: DOMINIC CLEMENTS - 9/17/2024 7:48:01 PM]

2.

Comment by Author: "Please add in post code SO16 7QF" 


[AUTHOR: DOMINIC CLEMENTS - 9/17/2024 7:48:11 PM]

3.

Comment by Author: "date should be 2020" 


[AUTHOR: DOMINIC CLEMENTS - 9/17/2024 8:28:26 PM]

4.

Comment by Author: "please change this citation to "Ying Chengjiong, Yang Wei and Yang Zhigang, Ground Viscous Effect on Stall of Wing in Ground Effect, 2010, The Third International Conference on Modelling and Simulation (ICMS2010), ISBN 978-1-84626-153-4, Wuxi, P.R.China, June. 4-6, 2010, pp.230-233" as my citaion software export the wrong names to the file." 

[AUTHOR: DOMINIC CLEMENTS - 9/17/2024 9:29:19 PM]

5.

Comment by Author: "url=
{https://api.semanticscholar.org/CorpusID:110018913}" 

[AUTHOR: DOMINIC CLEMENTS - 9/17/2024 9:59:39 PM]

6.

Comment by Author: "Please add this reference (picture cited from my other paper)"



[AUTHOR: DOMINIC CLEMENTS - 9/17/2024 10:13:03 PM]